The 2025 Asian Nuclear Physics Association board meeting and Symposium on Nuclear Physics facilities in Asia

The mechanisms of the complete, incomplete and quasifission processes in heavy ion collisions

Avazbek.K. Nasirov[1,2]

[1]Institute of Nuclear Physics, Academy of Science of Uzbekistan
[2]Bogoliubov Laboratory of Theoretical Physics, JINR , Dubna, Russia

Institute of Physics, Academia Sinica
November 29, 2025

Content

- Introduction
- Theoretical presentation of of reaction channels in heavy ion collisions at the around Coulomb barrier energies.
- Nature of hindrance in complete fusion of the massive nuclei in heavy ion collisions. Problems of the synthesis of superheavy elements heavier Z=118.
- Application of the new mechanism of the incomplete fusion to describe the measured data.

Conclusions.

Two different mechanisms of the complete fusion.

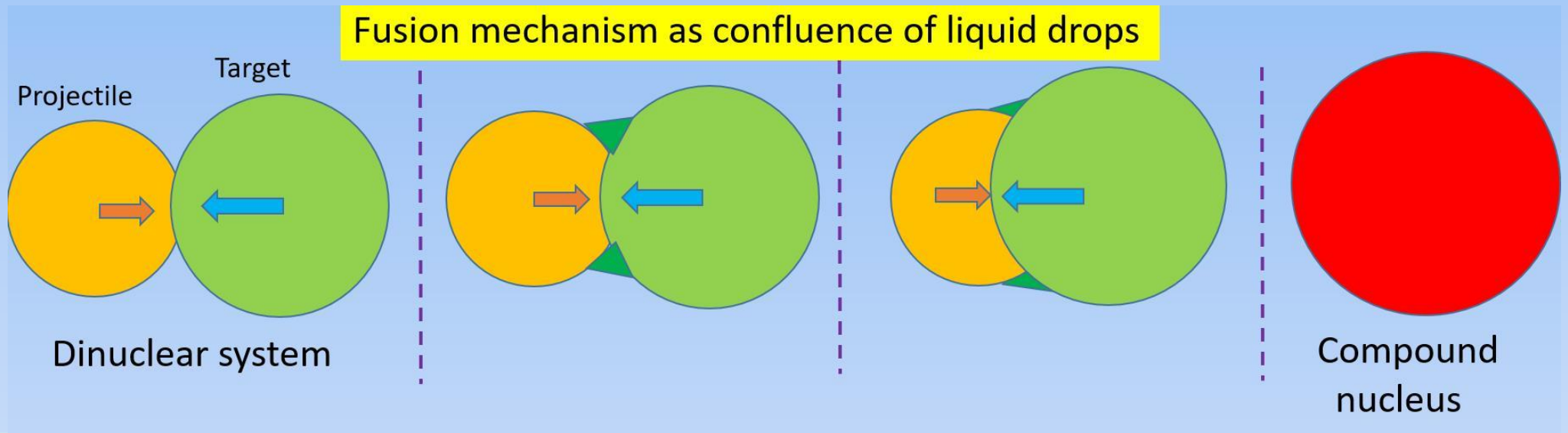

Multinucleon transfer mechanism of the complete fusion

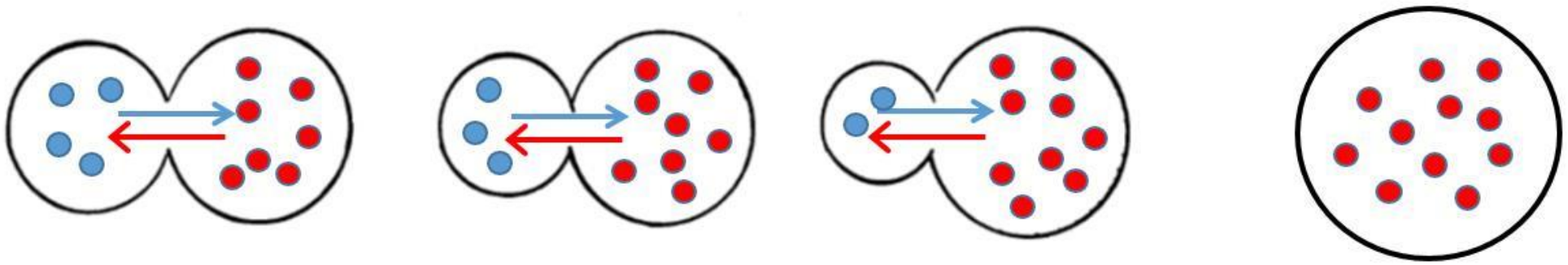

Two conceptions of the complete fusion

$$U(Z,A,R)=V_{\text{int}(Z,A)}+B_1(Z,A)+B_2(Z_{CN}-,A_{CN}-)-B_{\text{CN}}$$

N.V. Antonenko, et al. PRC 51, (1995) 2635. (Dinuclear system model)
G.G. Adamian et al. NPA 678 (2000) 24.
G. Giardina et al. EPJA 8, (2000) 205.

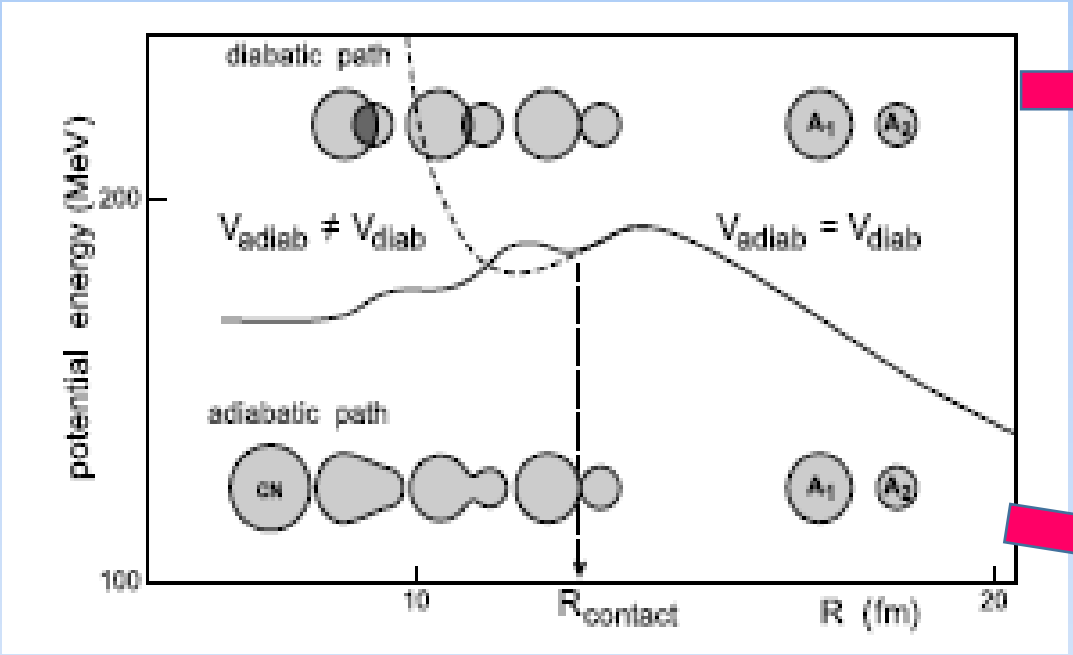

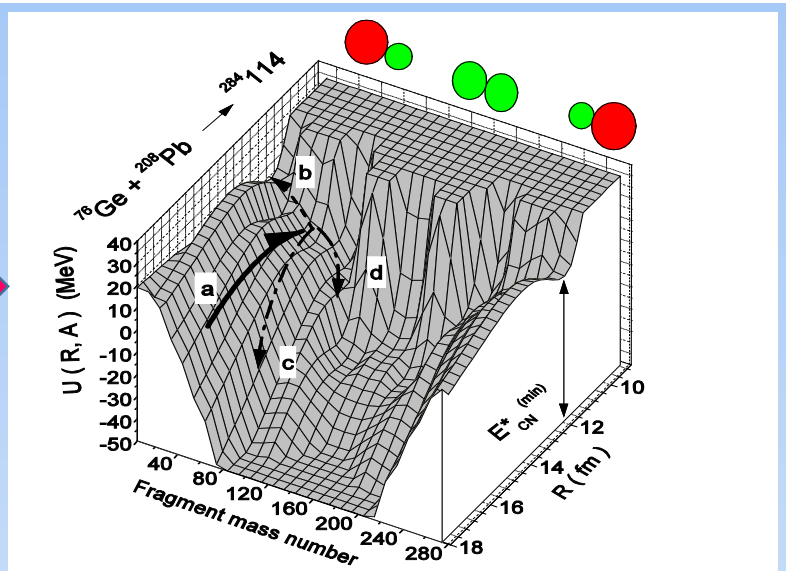

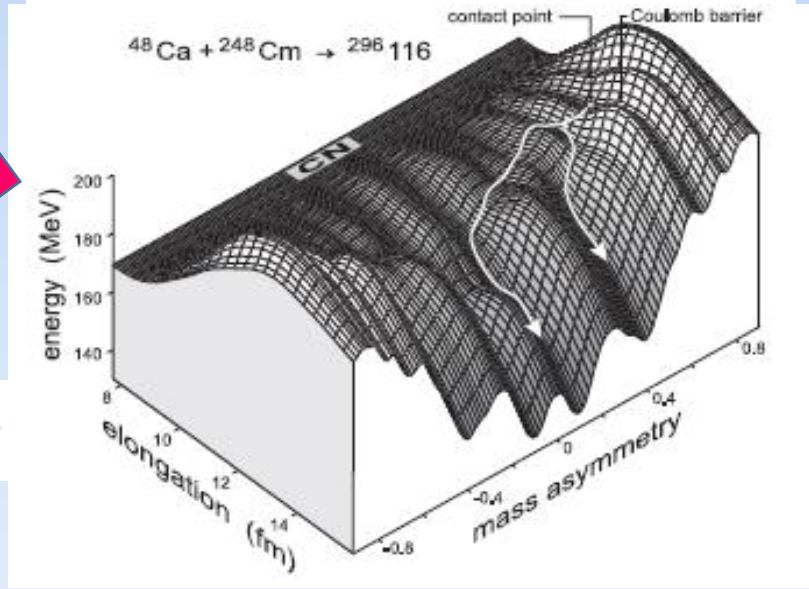

$$V = V_{\text{diab}}[1 - f(t)] + V_{\text{adiab}} f(t)$$

$$f(t = 0) = 0,\ f(t \gg \tau_{\text{relax}}) = 1.$$

$\tau_{\text{relax}} \sim 10^{-21}$ s (see, e.g., [24]),

[24] Bertsch G F 1978 *Z. Phys.* A **289** 103
Cassing W and Nörenberg W 1983 *Nucl. Phys.* A **401** 467

V. I. Zagrebaev, et al. J. Phys. G: Nucl. Part. Phys. **31** (2005) 825–844

Main reaction channels of the heavy ion collisions

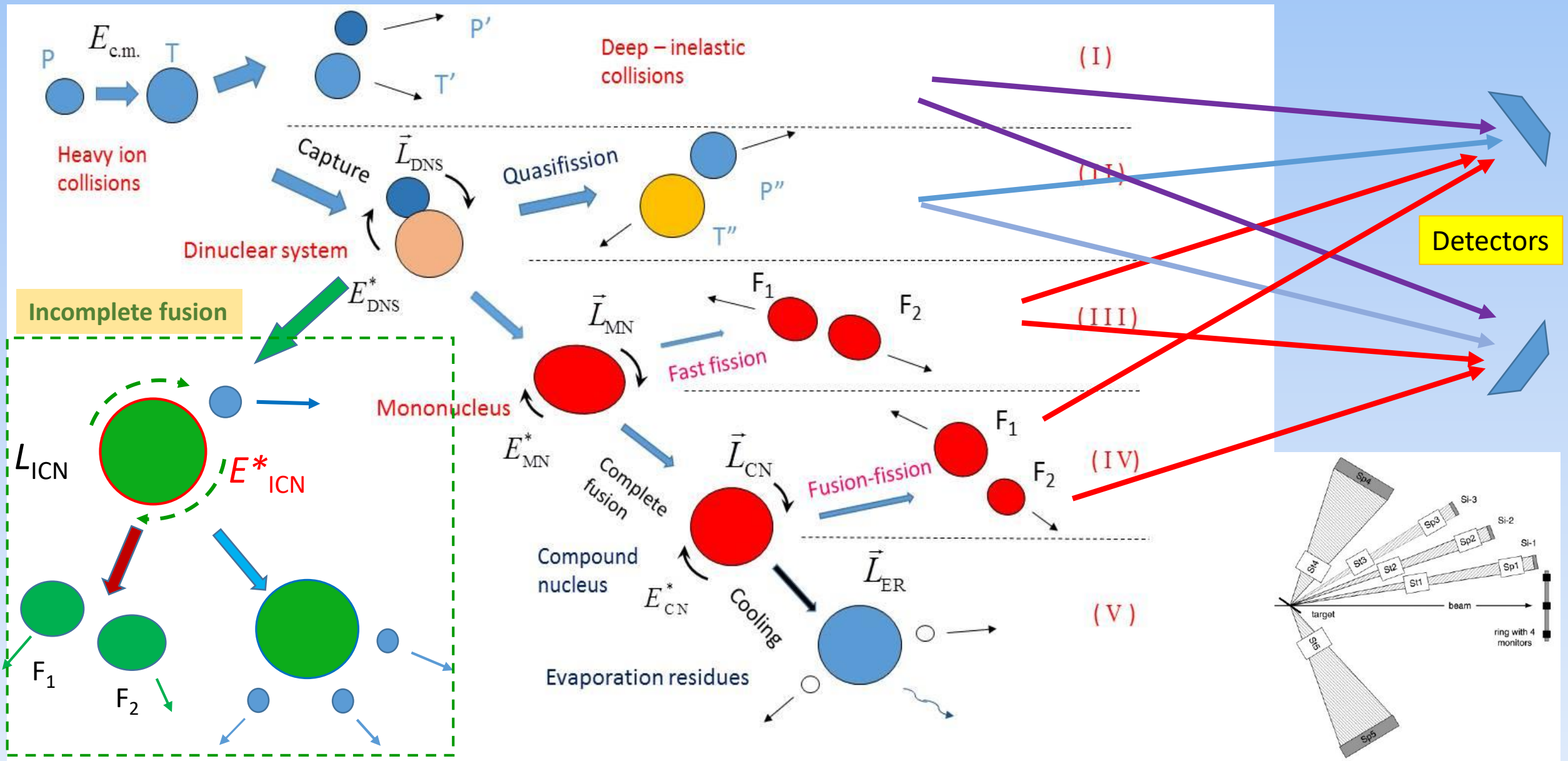

Main reaction channels of the heavy ion collisions

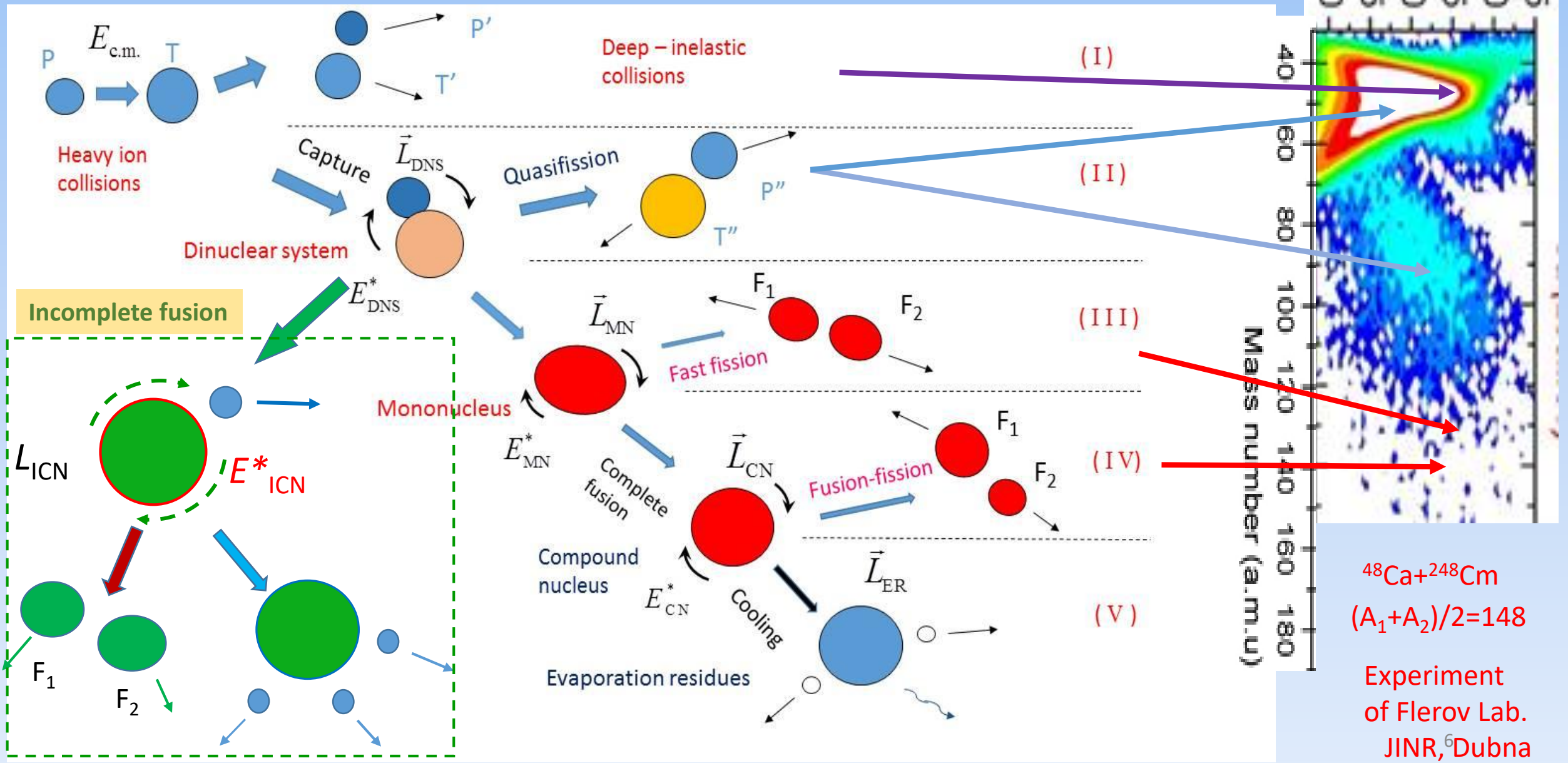

$^{48}Ca+^{248}Cm$

$(A_1+A_2)/2=148$

Experiment of Flerov Lab. JINR, Dubna

Association of the different mechanisms of the reaction channels with potential energy surface of the dinuclear system formed at capture.

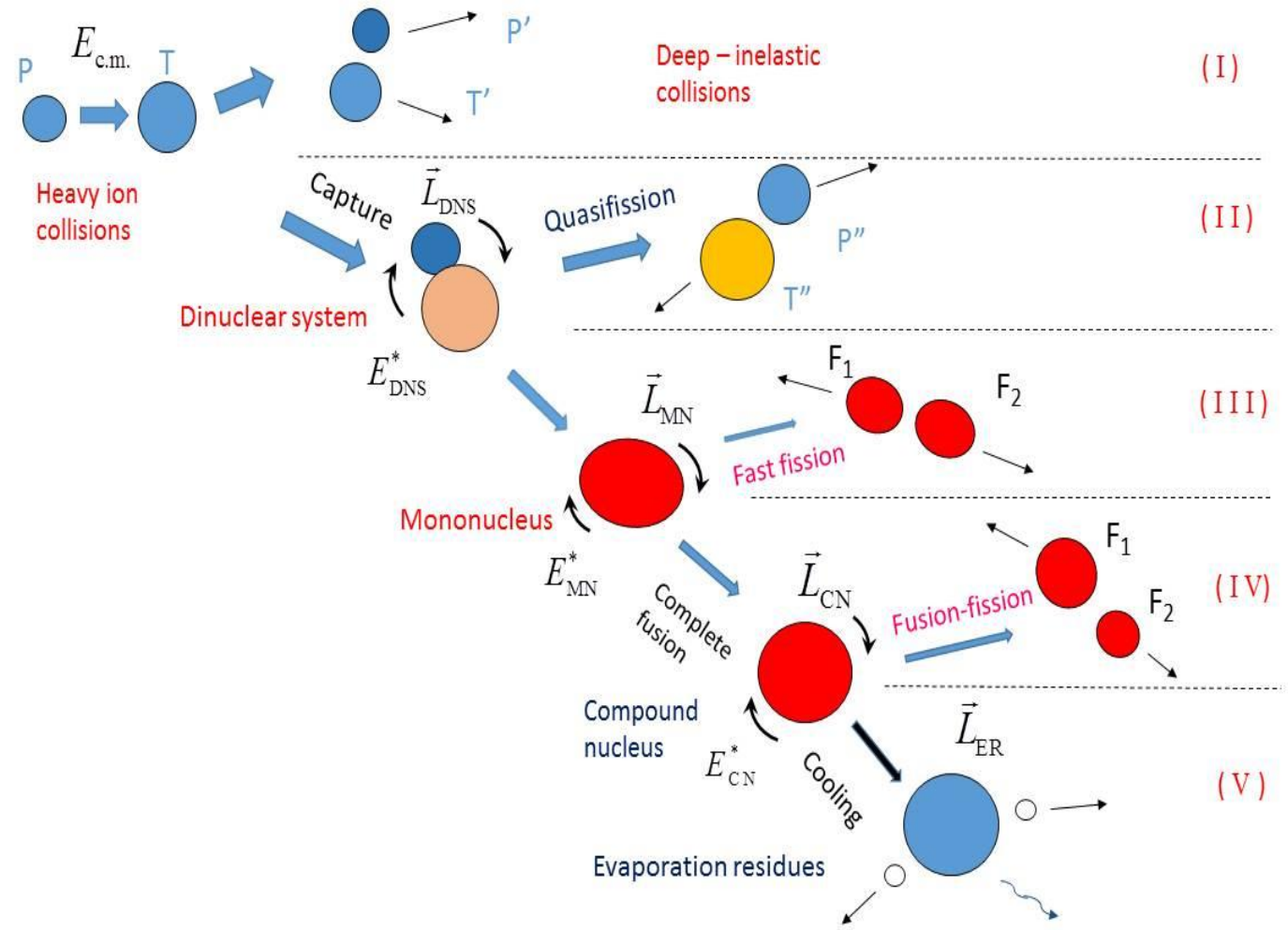

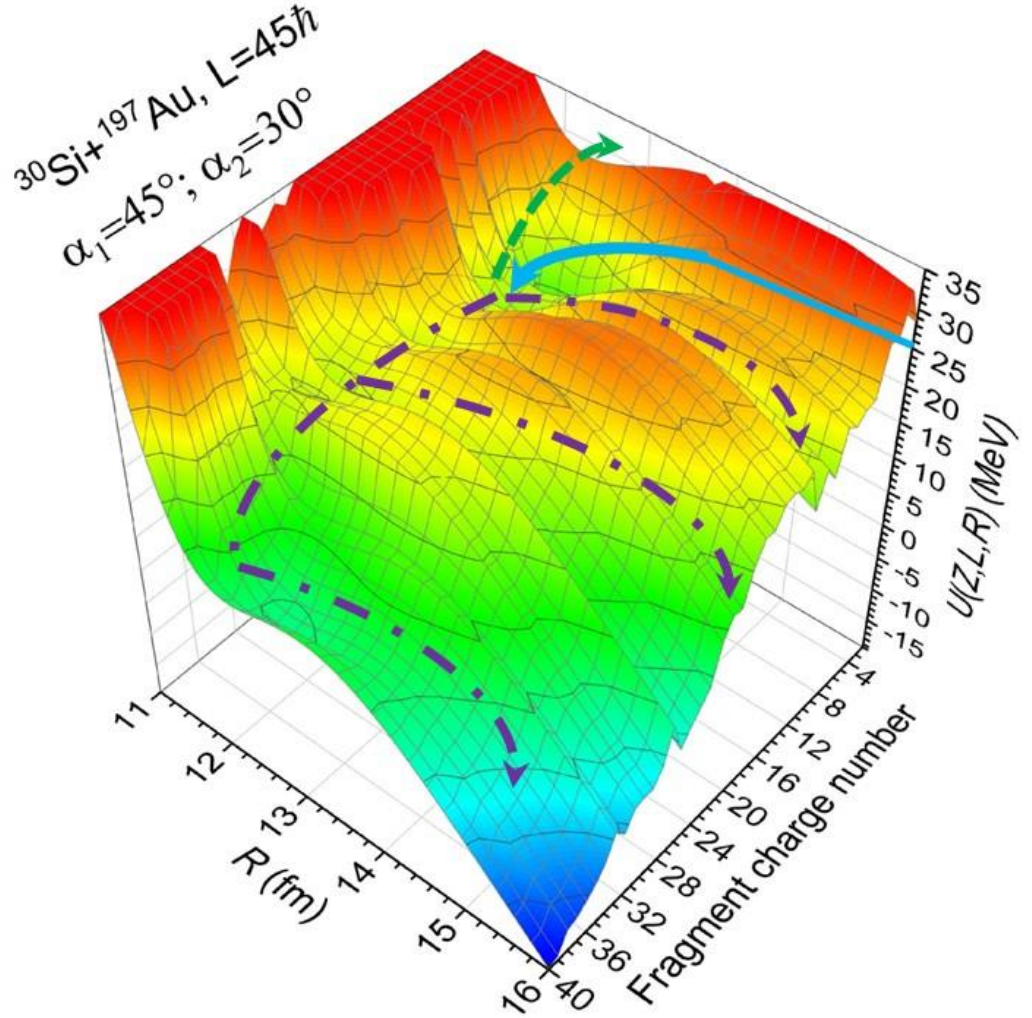

- Reactions leading to synthesis of superheavy elements.

Quasifission and fusion-fission in reactions with massive nuclei: Comparison of reactions leading to the Z = 120 element

A.K. Nasirov, *et al*. Phys. Rev. C 79, 024606 (2009).

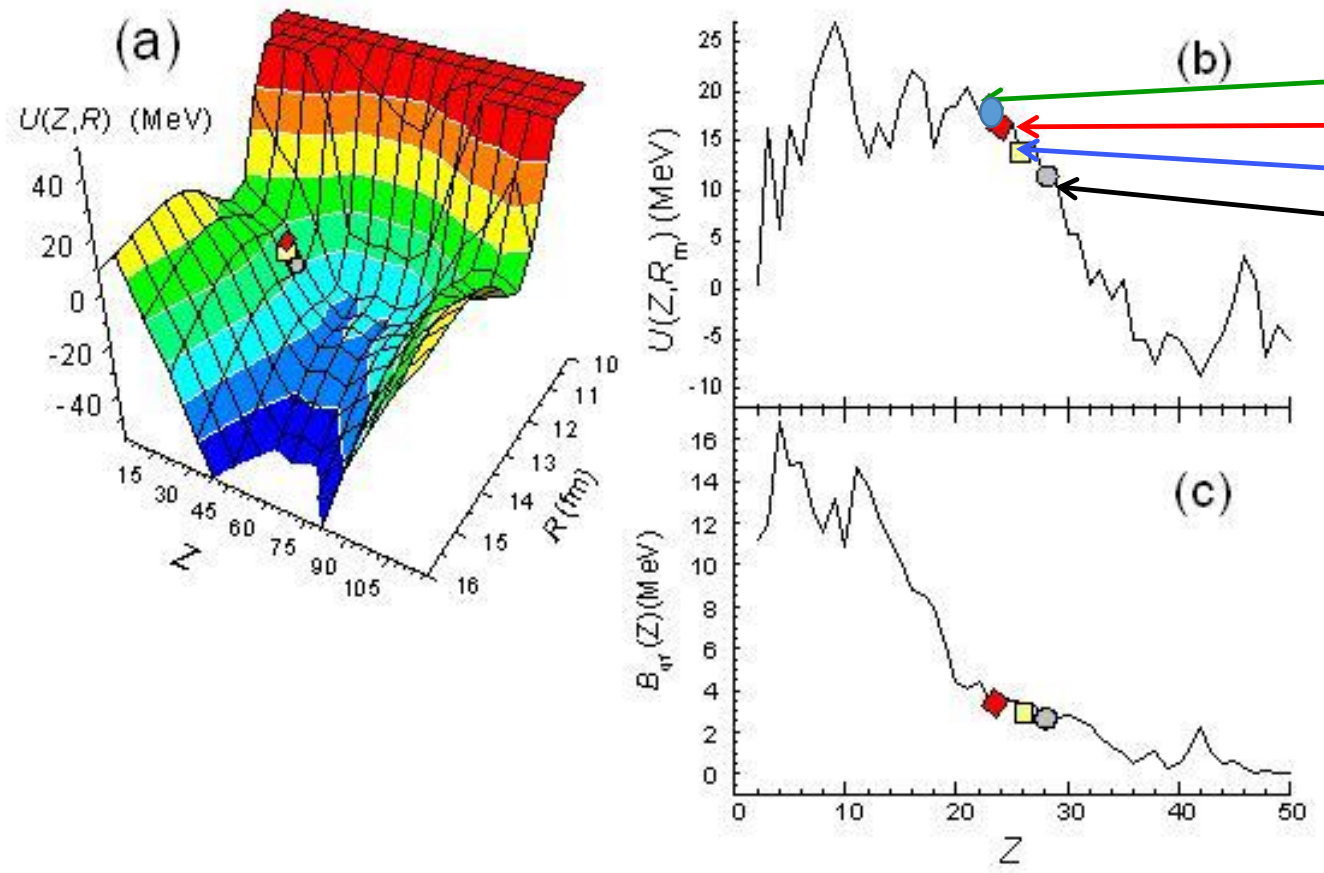

50Ti + 249Cf
54Cr + 248Cm
58Fe + 244Pu
64Ni + 238U

Reactions	$E_{c.m.}$(MeV)	Evaporation residues cross section (pb)
50Ti + 249Cf	225	4×10^{-2}
54Cr + 248Cm	236	2×10^{-3}
58Fe + 244Pu	252	7×10^{-4}
64Ni + 238U	275	2×10^{-6}

Differences in the cross sections of the evaporation residues of the same superheavy elements, obtained for cold and hot fusion reactions, shows the dependence of the fission barrier on neutron numbers.

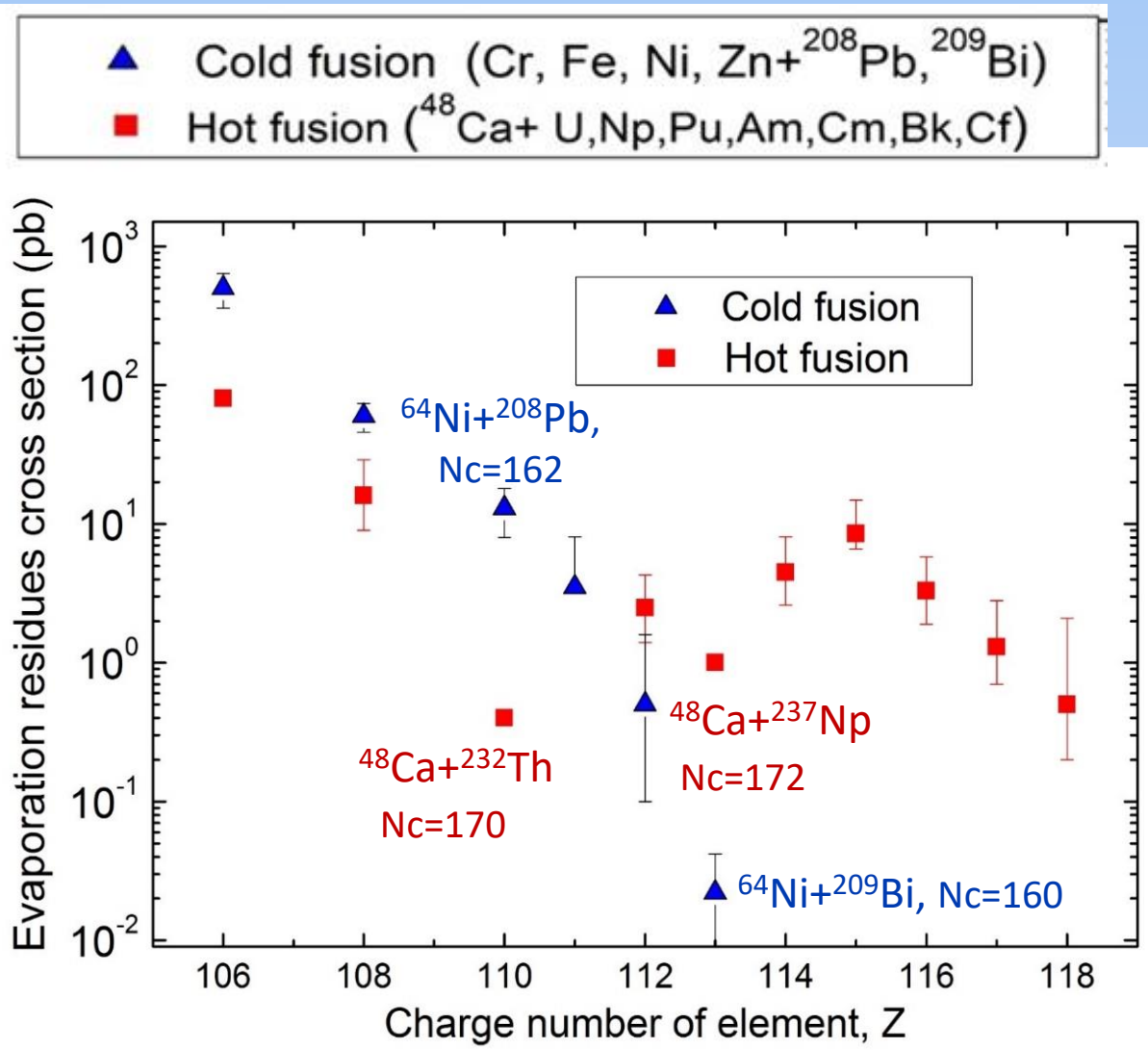

Fission barrier of the superheavy elements as a function of their neutron numbers.

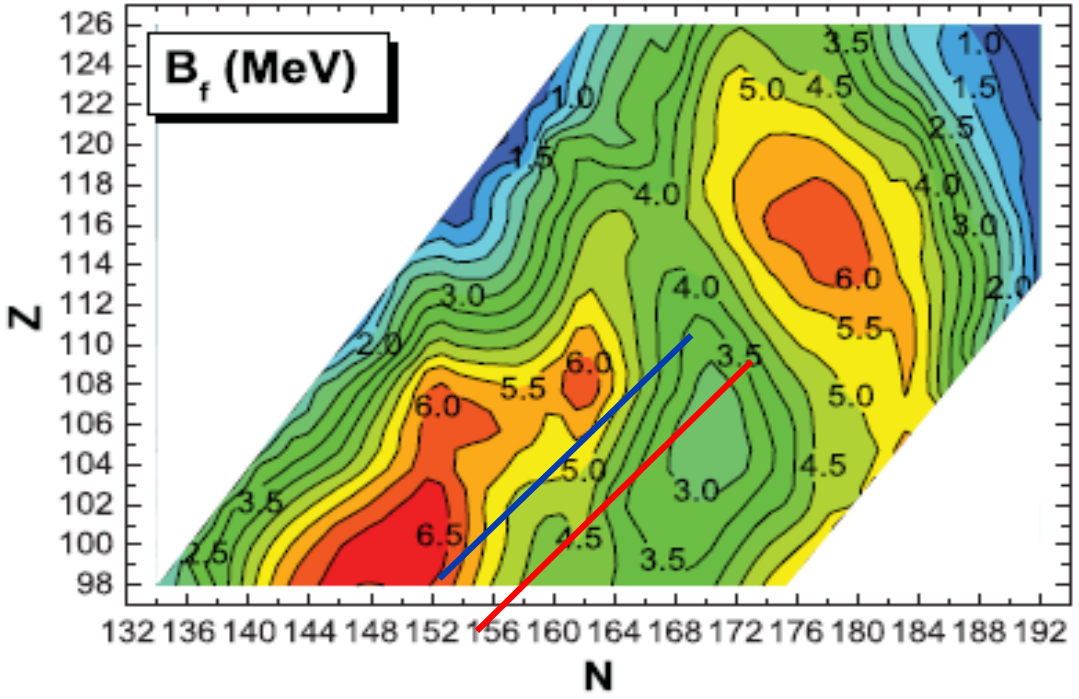

FIG. 6. (Color online) Contour map of calculated fission barrier heights B_f for even-even superheavy nuclei.

M. Kowal et al, Phys. Rev. C **82**, 014303 (2010).

Differences in the cross sections of the evaporation residues of the same superheavy elements, obtained for cold and hot fusion reactions, shows the dependence of the fission barrier on neutron numbers.

PHYSICAL REVIEW C **110**, 014618 (2024)
A.K.N., A. R. Yusupov, and B. M. Kayumov. **Small cross section of the synthesis of darmstadtium in the $^{48}Ca+^{232}Th$ reaction.**

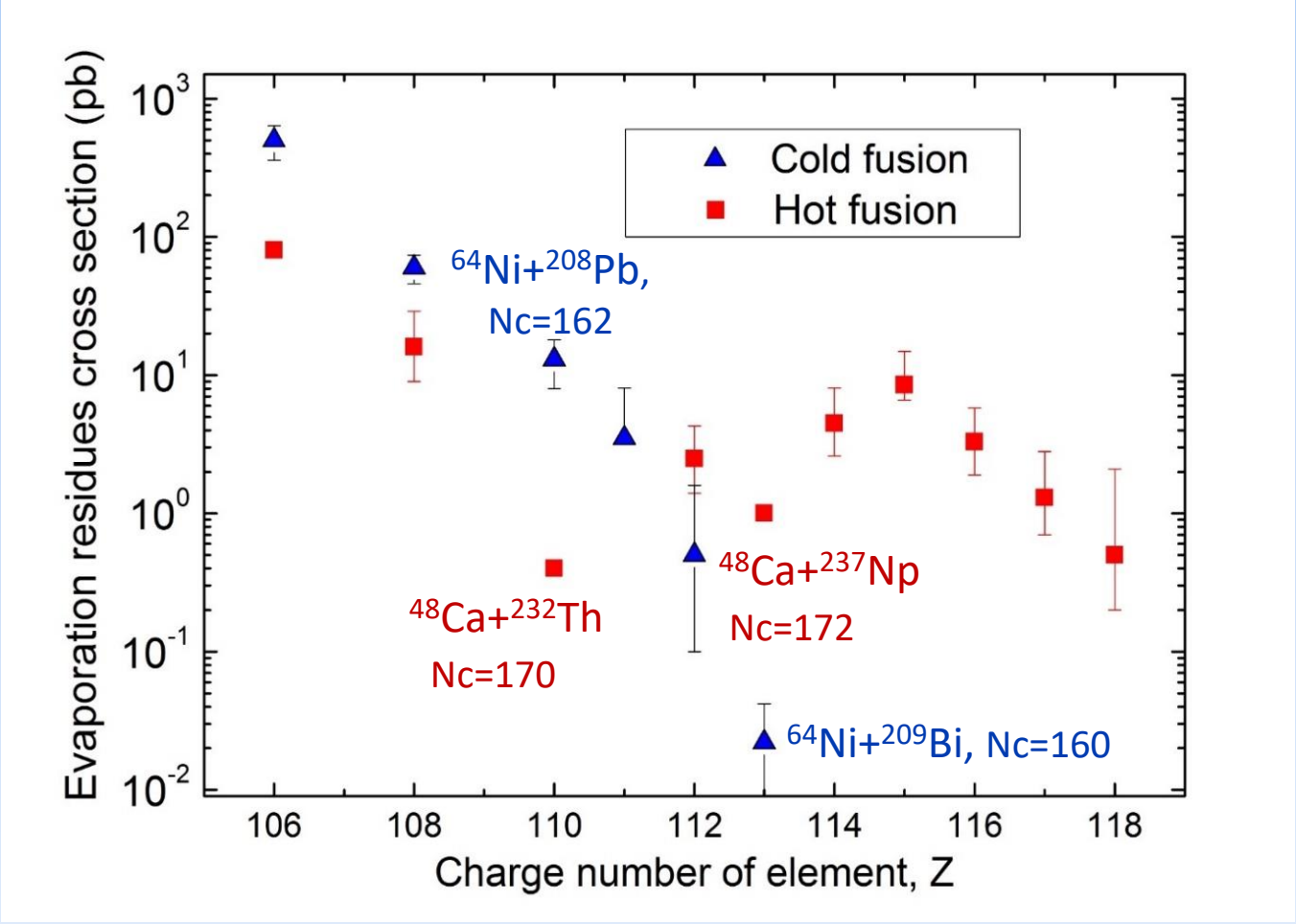

Fission barrier of the superheavy elements as a function of their neutron numbers.

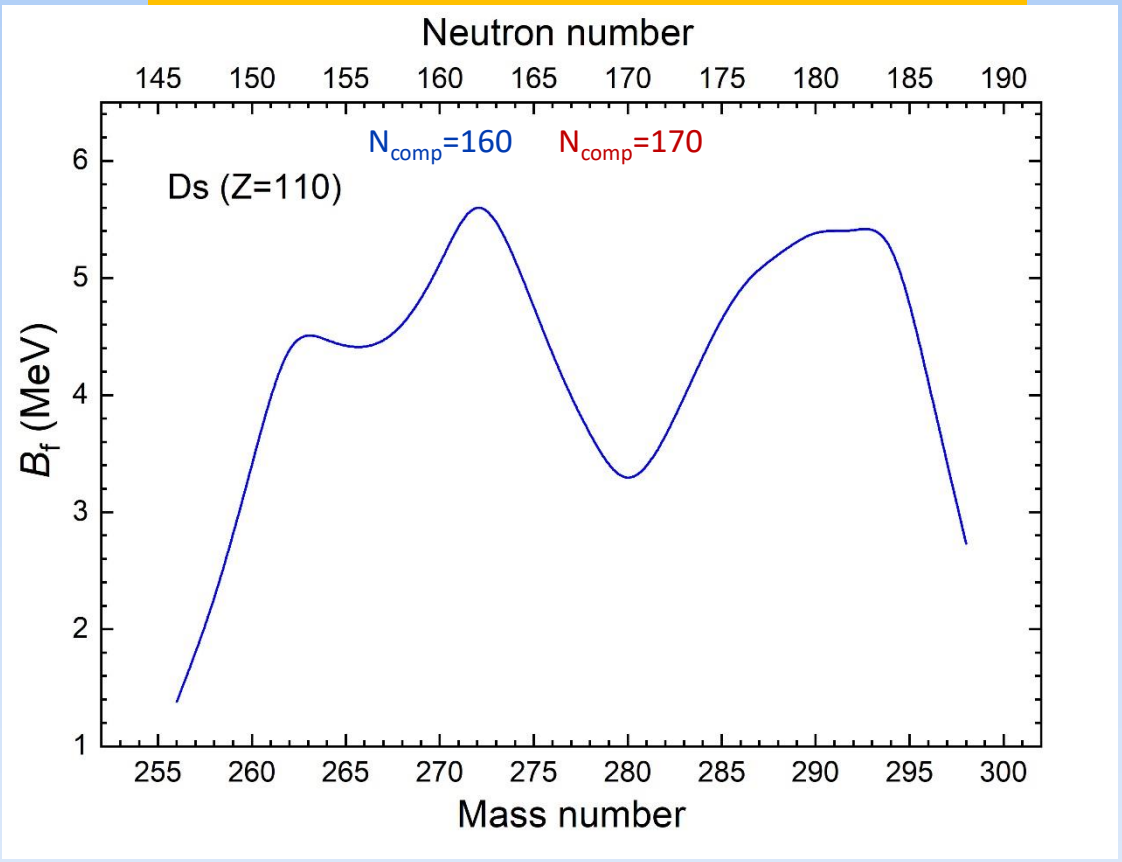

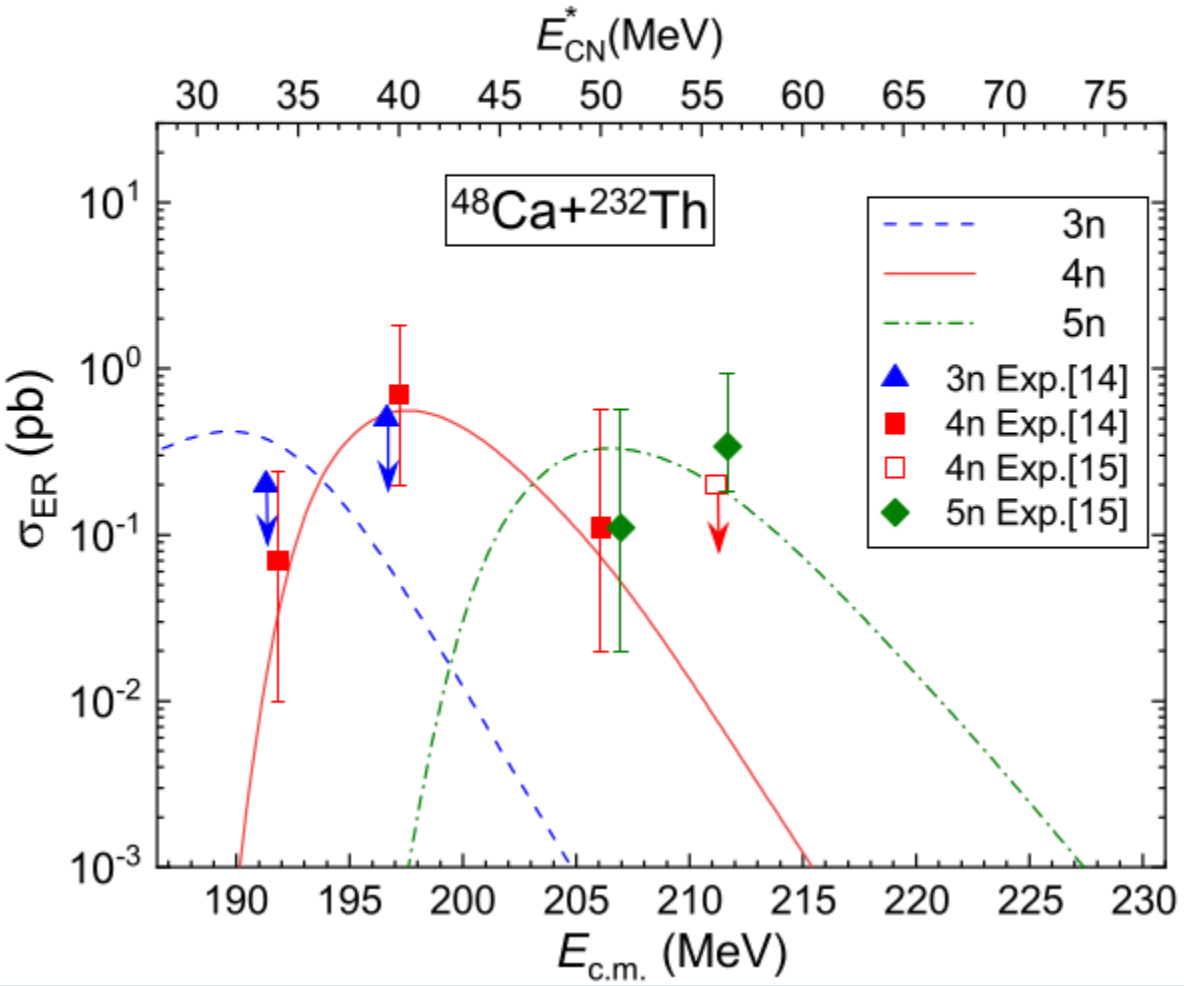
E^*_{CN}(MeV)
30 35 40 45 50 55 60 65 70 75
^{48}Ca+^{232}Th
3n
4n
5n
3n Exp.[14]
4n Exp.[14]
4n Exp.[15]
5n Exp.[15]
σ_{ER} (pb)
10^1 10^0 10^{-1} 10^{-2} 10^{-3}
190 195 200 205 210 215 220 225 230
$E_{c.m.}$ (MeV)

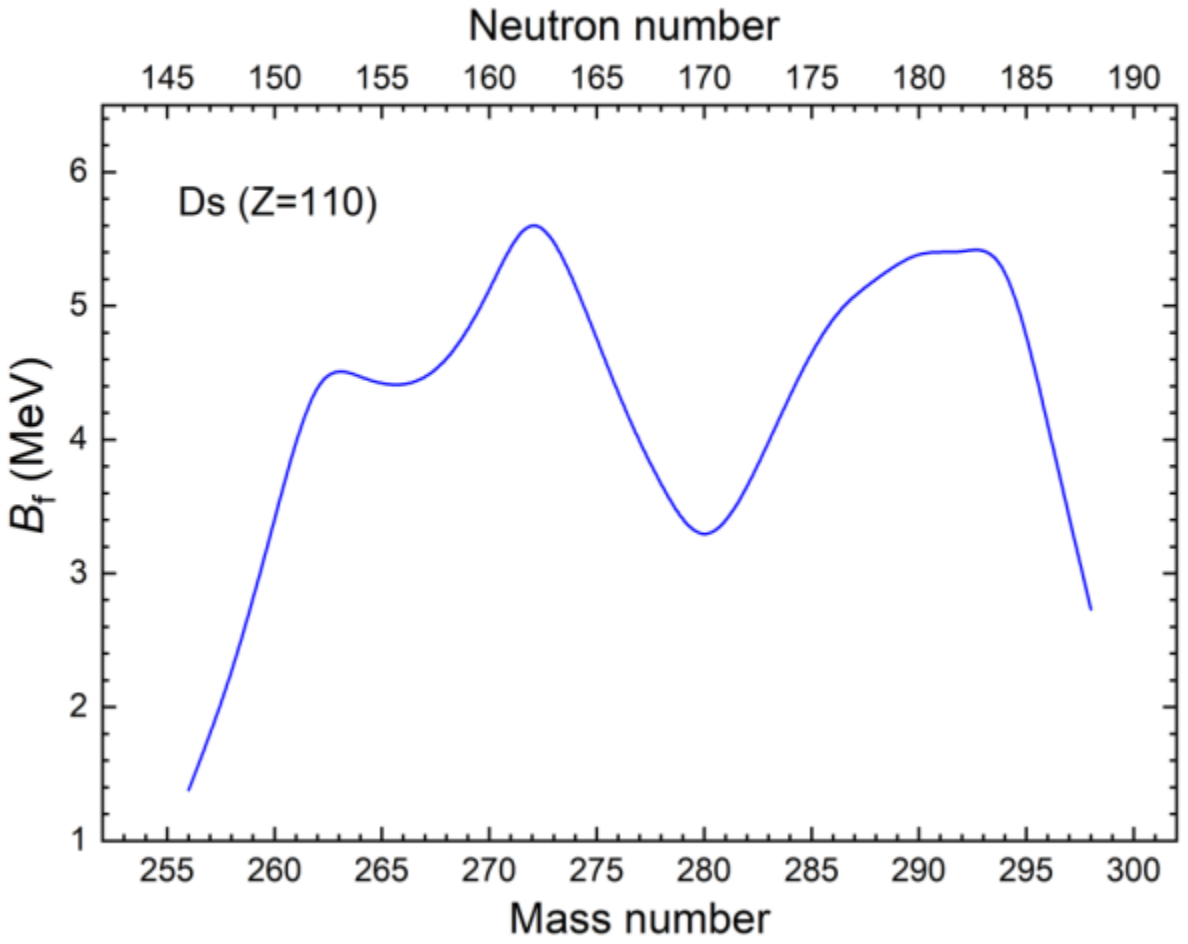
Neutron number
145 150 155 160 165 170 175 180 185 190
Ds (Z=110)
B_f (MeV)
1 2 3 4 5 6
255 260 265 270 275 280 285 290 295 300
Mass number

Influence of the rotational energy of the dinuclear system on the nucleon transfer process.

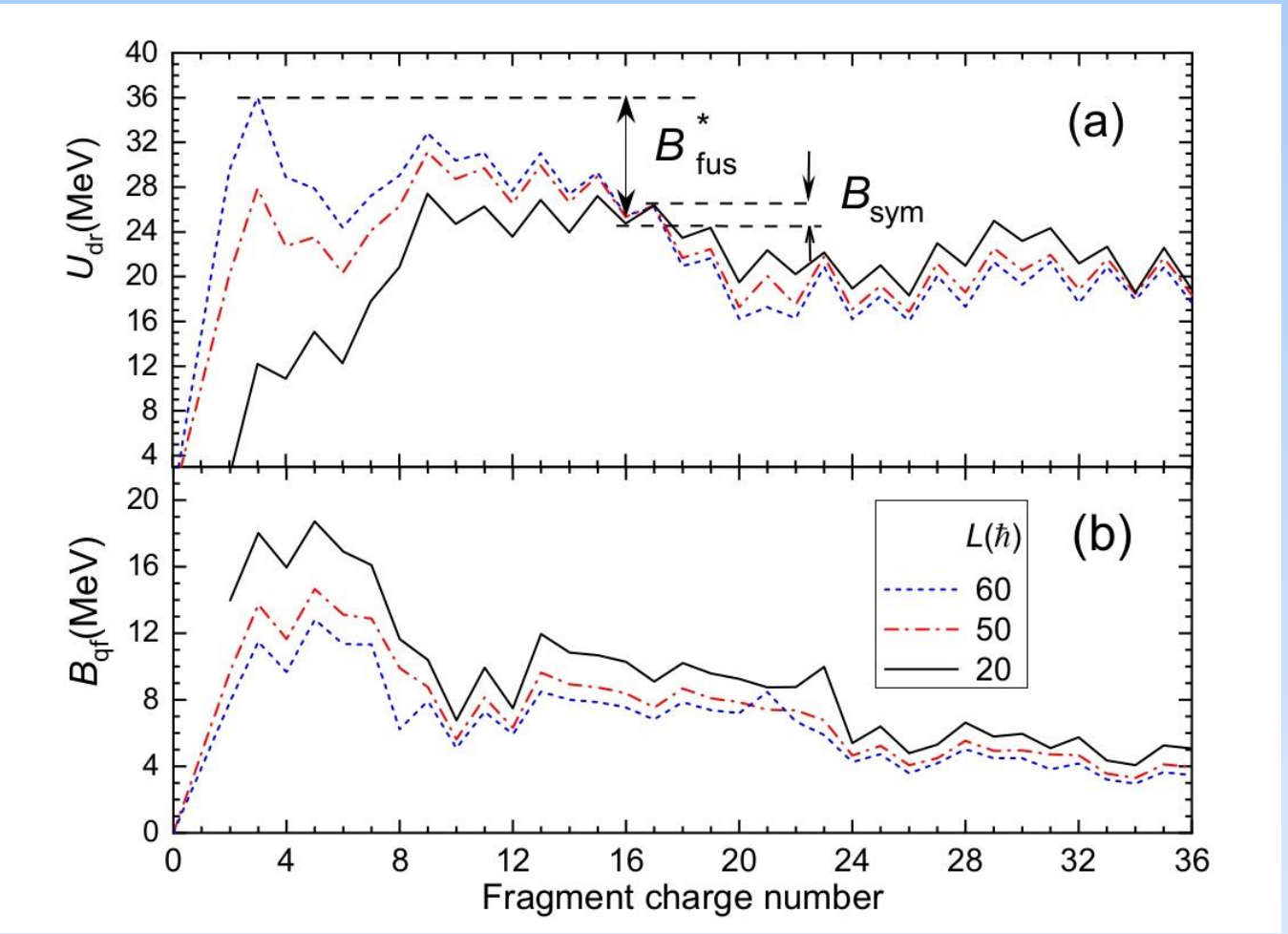

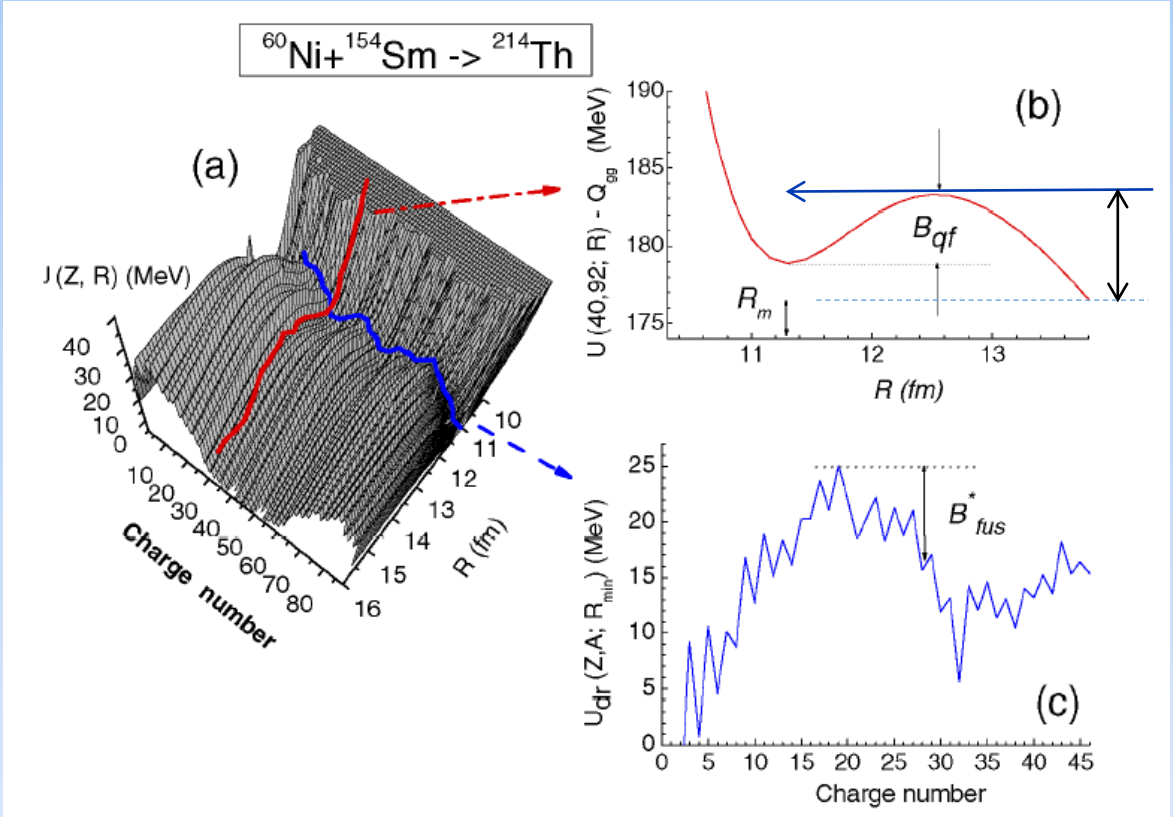

Reasons causing a difference in the synthesis of the superheavy elements in the cold and hot complete fusion channels.

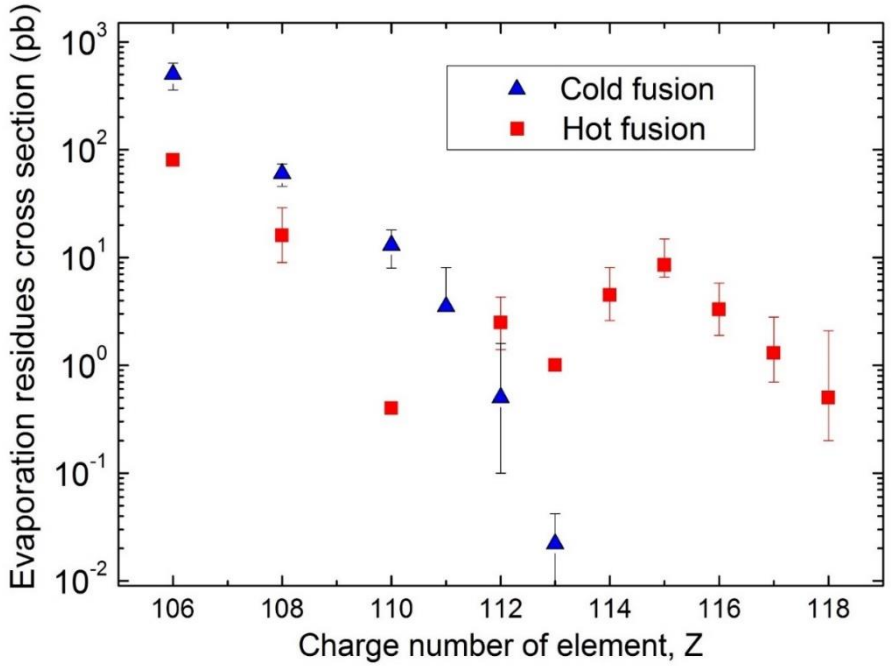

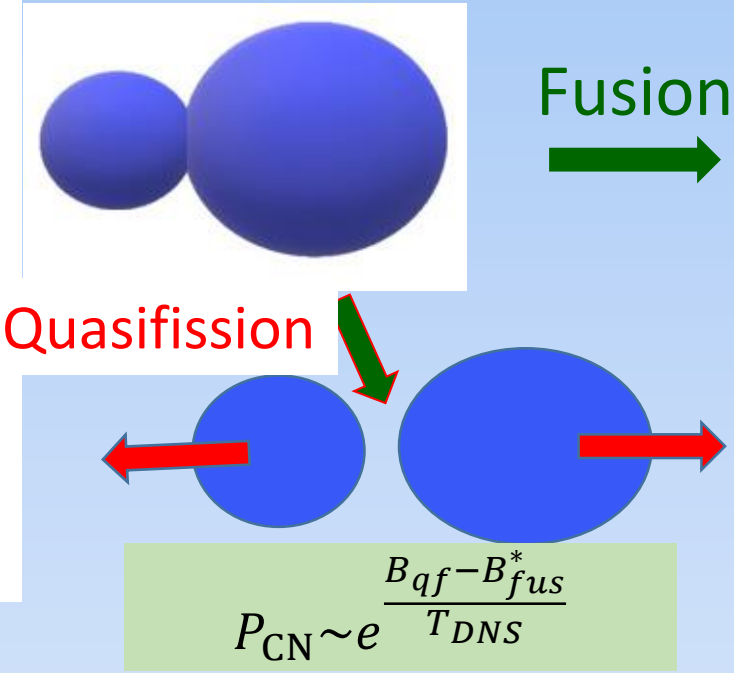

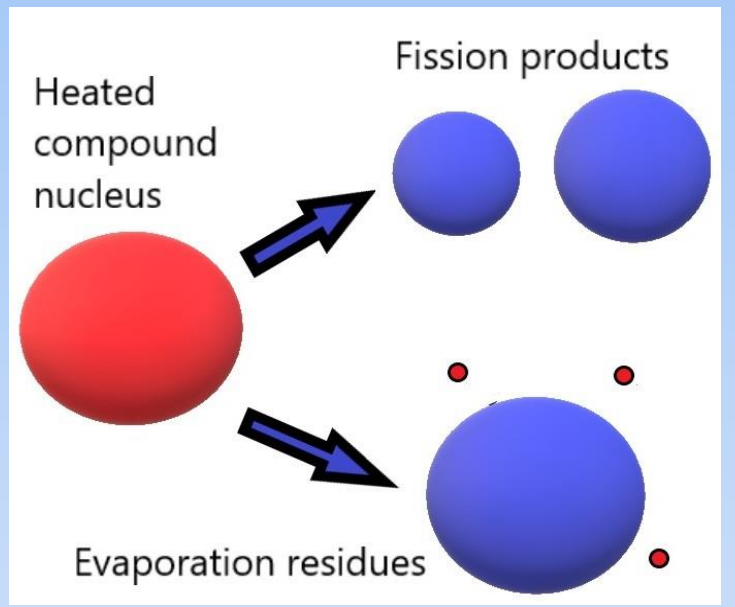

$$P_{\mathrm{CN}} \sim e^{\frac{B_{qf}-B^{*}_{fus}}{T_{DNS}}}$$

$$W_{\mathrm{surv}} \sim e^{\frac{B_{fis}-B_{n}}{T_{CN}}}$$

$$\sigma_{ER}(E^{*}) = \sum_{\ell=0}^{\ell=\ell_f} \sigma_{\mathrm{cap}}(E_{\mathrm{c.m.}}, \ell) P_{\mathrm{CN}}(E^{*}_{DNS}, \ell) W_{\mathrm{surv}}(E_{CN}{}^{*}, \ell)$$

P_{CN} (cold fusion) $\ll P_{\mathrm{CN}}$(hot fusion)

W_{surv} (cold fusion) $\gg W_{\mathrm{surv}}$(hot fusion)

B^{*}_{fus} (cold fusion) > B^{*}_{fus} (hot fusion)

B_{fis} (cold fusion) > B_{fis} (hot fusion)

N.V. Antonenko, et al. PRC 51, (1995) 2635.
G.G. Adamian et al. NPA 678 (2000) 24.
G. Giardina et al. EPJA 8, (2000) 205.

Role of the potential energy surface in calculation of the fusion probability.

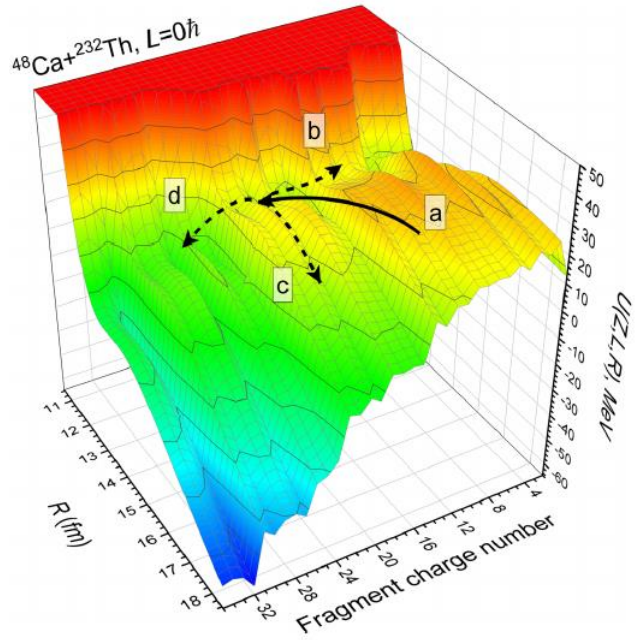

FIG. 3. The potential energy surface of the DNS formed in the reaction $^{48}\mathrm{Ca}+^{232}\mathrm{Th}$ calculated for collisions with the value of the orbital angular momentum $\ell = 0$ and the orientation angles $\alpha_1 = 30^\circ$ and $\alpha_2 = 135^\circ$. The arrow (a) shows the input capture channel; the arrow (b) shows the directions of the complete fusion by the nucleon transfer from a light nucleus to a heavy one; arrows (c) and (d) show the directions of the DNS decay into mass-asymmetric and symmetric quasifission channels, respectively.

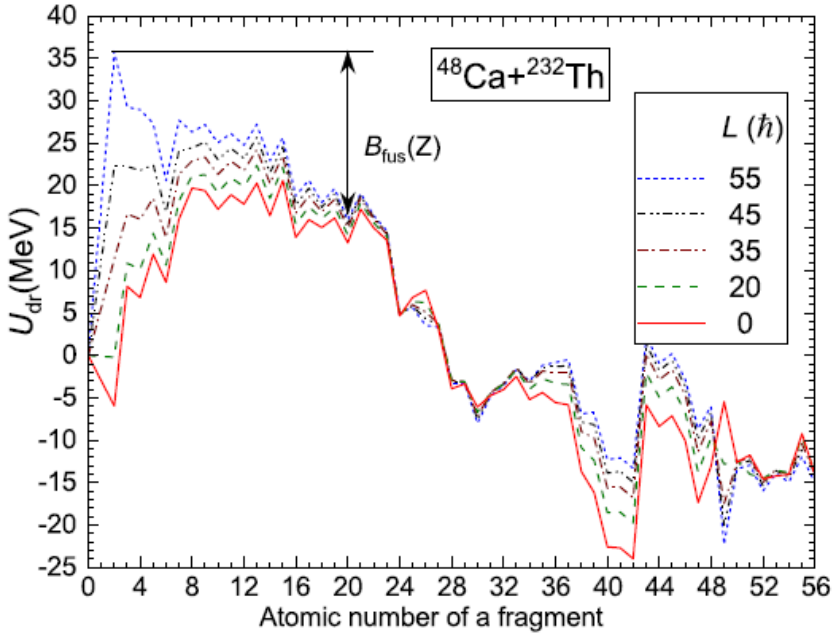

FIG. 4. The driving potential calculated for the $^{48}\mathrm{Ca}+^{232}\mathrm{Th}$ reaction for the orientation angles $\alpha_P = 30^\circ$ and $\alpha_T = 45^\circ$ of the axial symmetry of the nuclei of DNS formed with the angular momentum $L = 0, 20, 35, 45, 55\ \hbar$. $B^*_{fus}(Z)$ is an internal nuclear barrier that causes hindrance to complete fusion for the charge asymmetry state $Z = 20$ of the DNS.

$$\sigma_{\mathrm{fus}}(E_{\mathrm{c.m.}}, \ell) = \int_0^{\pi/2} \sigma_{\mathrm{cap}}(E_{\mathrm{c.m.}}, \ell, \alpha_T) P_{CN}(E_{\mathrm{c.m.}}, \ell, \alpha_T) \sin\alpha_T d\alpha_T$$

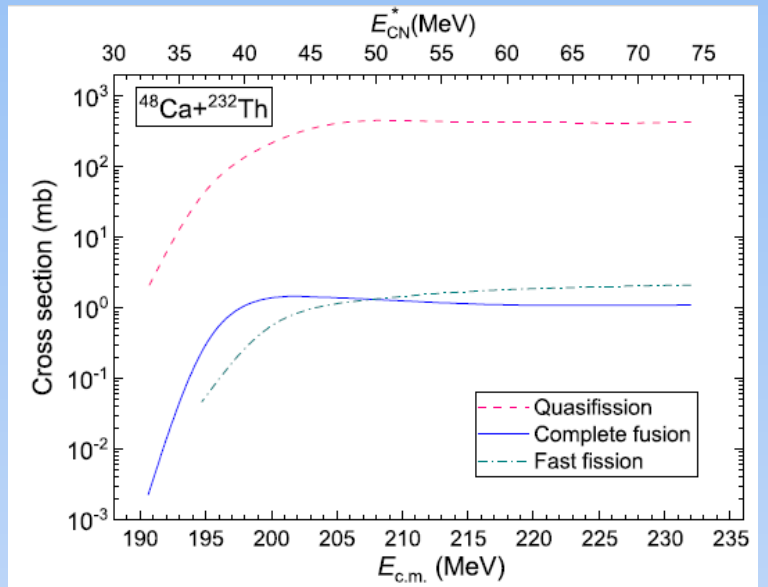

FIG. 7. Cross sections of the quasifission (dashed curve), complete fusion (solid curve), and fast fission (dot-dashed curve) calculated in this work for the reaction $^{48}\mathrm{Ca}+^{232}\mathrm{Th}$.

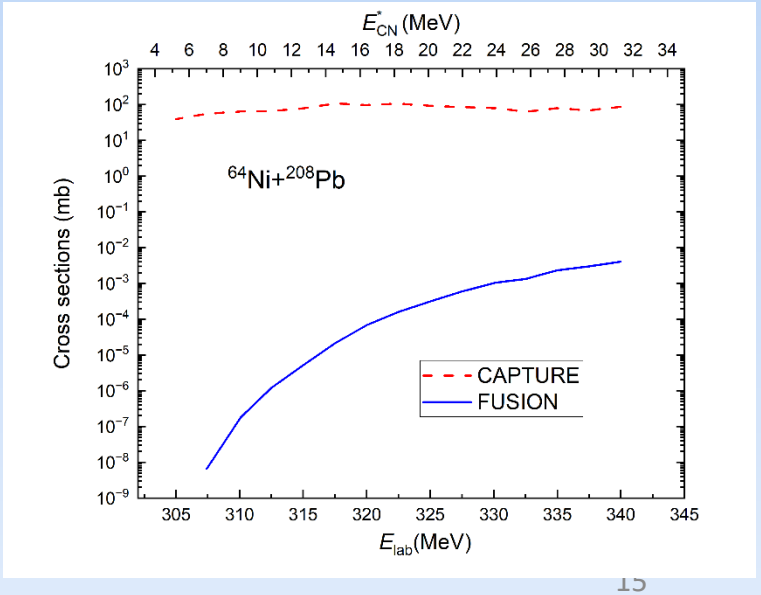

Calculation of the competition between complete fusion and quasifission: $P_{cn}(E_{DNS},L)$

$$P_{CN}(E^*_{DNS},\ell)=\sum_{Z_{sym}}^{Z_{max}} Y_Z(E^*_{DNS},\ell)P^{(Z)}_{CN}(E^*_{DNS},\ell)$$

where

$$P^{(Z)}_{CN}(E^*_{DNS},\ell)=\frac{\rho(E^*_{DNS}(Z)-B^*_{fus}(Z),\ell)}{\rho(E^*_{DNS}(Z)-B^*_{fus}(Z),\ell)+\rho(E^*_{DNS}(Z)-B^*_{qf}(Z),\ell)+\rho(E^*_{DNS}(Z)-B^*_{sym}(Z),\ell)}$$

$$E^*_{DNS}(Z)=E_{c.m.}-V_{min}(Z)+(B_P+B_T)-(B_Z+B_{Ztot-Z})$$

$$\frac{\partial}{\partial t}Y_Z(E^*_Z,\ell,t)=\Delta^{(-)}_{Z+1}Y_{Z+1}(E^*_Z,\ell,t)+\Delta^{(+)}_{Z-1}Y_{Z-1}(E^*_Z,\ell,t)$$

$$-(\Delta^{(-)}_Z+\Delta^{(+)}_Z+\Lambda^{qf}_Z)Y_Z(E^*_Z,\ell,t)$$

$$\text{for } Z=2,3,\ldots,Z_{tot}-2$$

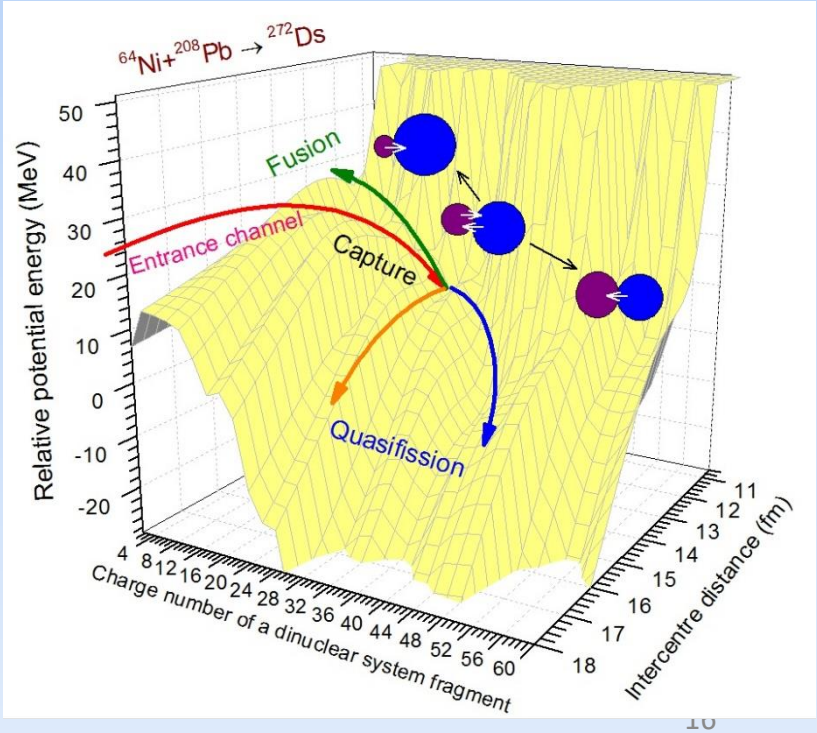

Nasirov A.K. et al. Nuclear Physics A 759 (2005) 342–369

Fazio G. et al, Modern Phys. Lett. A 20 (2005) p.391

Nasirov A.K. et al. Phys. Rev. C 110, 014618 (2024)

Main characteristics of the entrance channel of the nuclear reactions

- Total mass and charge number of the colliding nuclei.
- Charge and mass asymmetry of the colliding nuclei ($Z_1<Z_2$ or $Z_1 \sim Z_2$).
- Ratio of the mass and charge numbers A_1/Z_1 and A_2/Z_2 .
- Beam energy E_{lab} and orbital angular momentum $\vec{L} = [\vec{b} \times \vec{P}]$.
- Orientation angles of the symmetry axis of the deformed nuclei.
- Microscopic shell structure of nuclei.

The difference in the evaporation residues (ER) of the $^{34}S + ^{208}Pb$ and $^{36}S + ^{206}Pb$ reactions formed in the 2n and 3n channels has been explained by two reasons:

i) the capture cross section of the $^{36}S + ^{206}Pb$ reaction is larger than the one of the $^{34}S + ^{208}Pb$ reaction since the nucleus-nucleus potential is more attractive in the $^{36}S + ^{206}Pb$.

Ii) the intrinsic fusion barrier B^*_{fus} for the $^{34}S + ^{208}Pb$ reaction is higher than the one obtained for the $^{36}S + ^{206}Pb$ reaction.

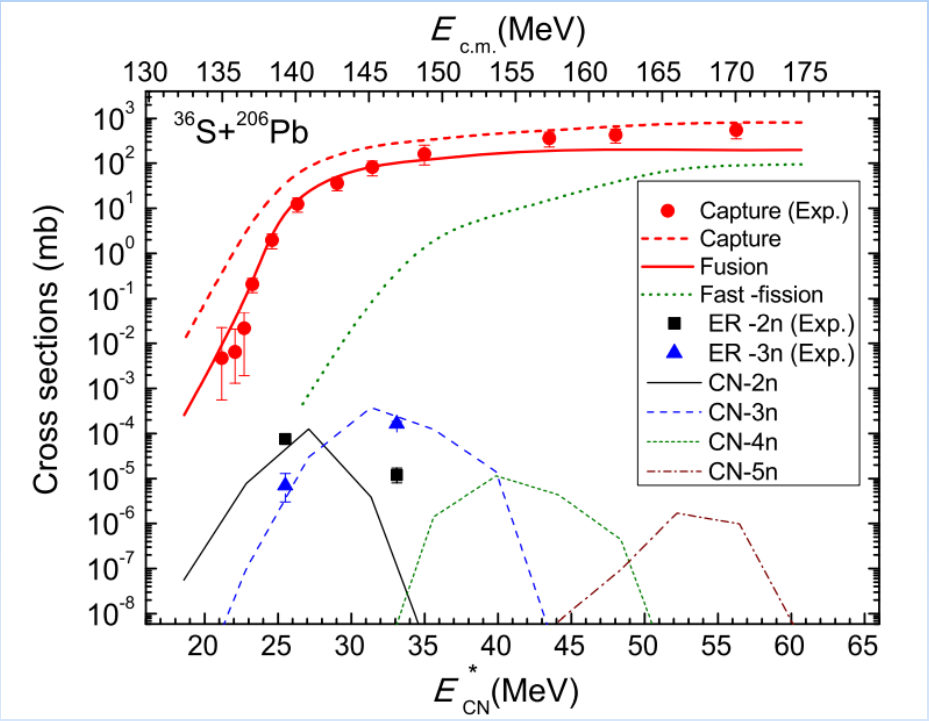

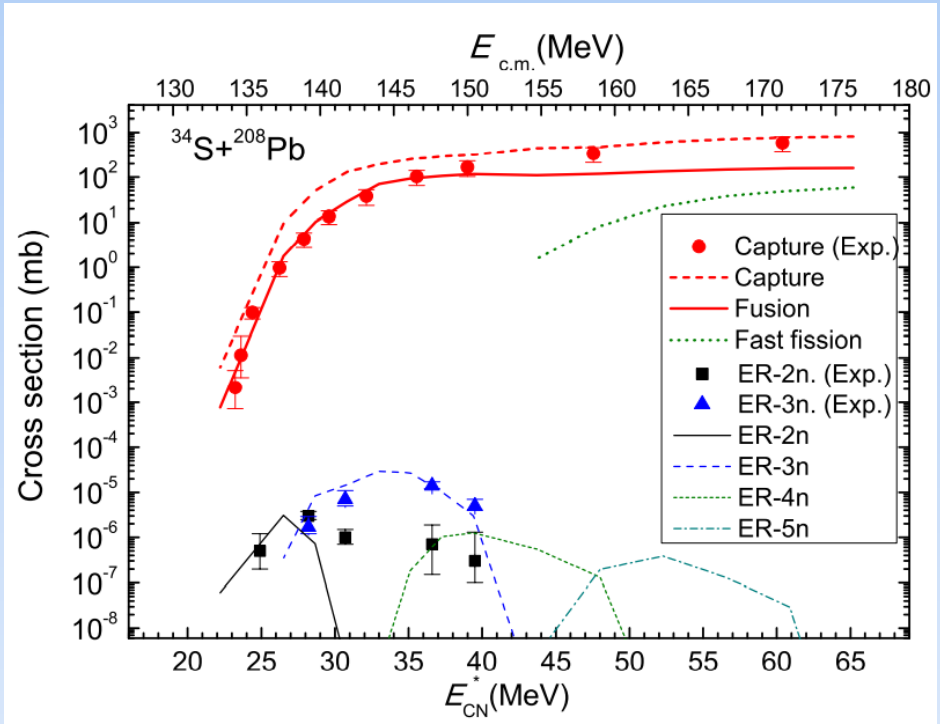

Experiment (symbols)

1. J. Khuyagbaatar *et al*, Phys. Rev. C 86, 064602 (2012)

2. J. Khuyagbaatar *et al*, Phys. Rev. C 91, 054608 (2015).

Theory (curves)

A.K. Nasirov *et al*. Eur. Phys. J. A (2019) 55: 29

Role of the non-equilibrium stage of the entrance channel in formation of the compound nucleus.

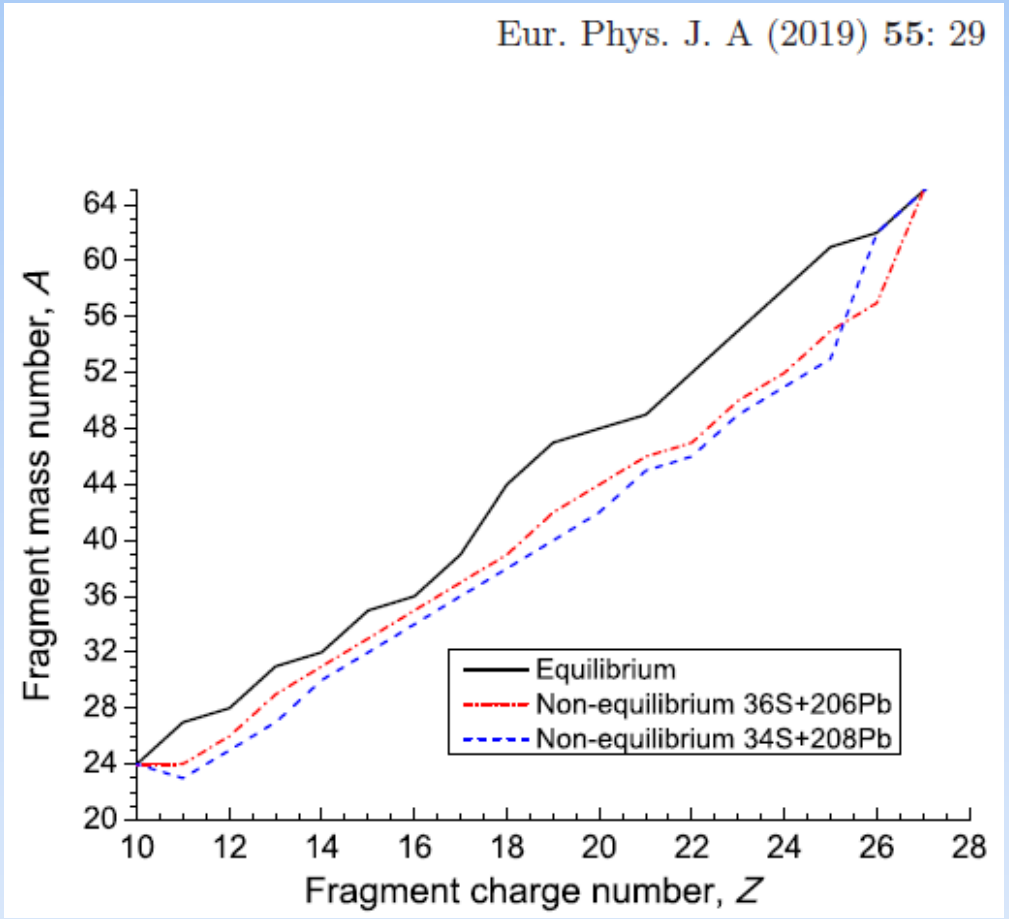

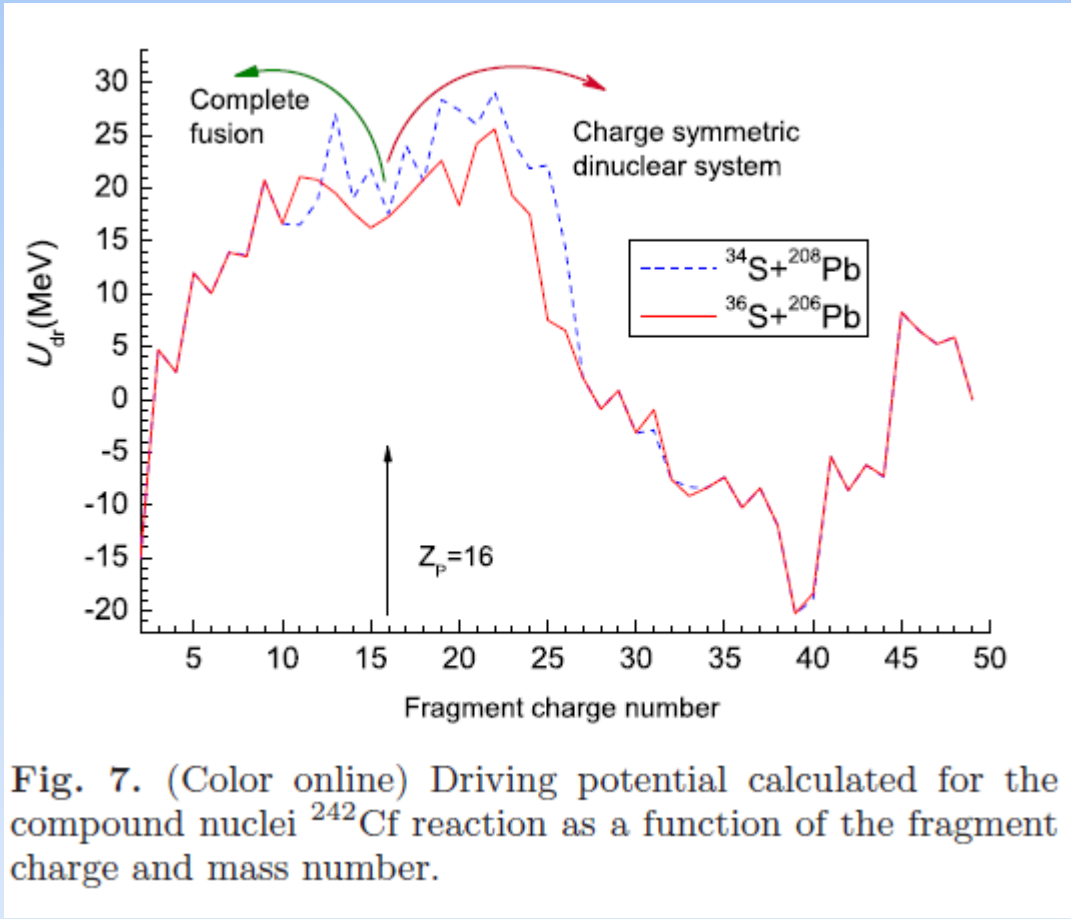

Fig. 7. (Color online) Driving potential calculated for the compound nuclei ^{242}Cf reaction as a function of the fragment charge and mass number.

Comparison of the potential energy surfaces ruling complete fusion in the of $^{34}S+^{208}Pb$ and $^{36}S+^{206}Pb$ reactions

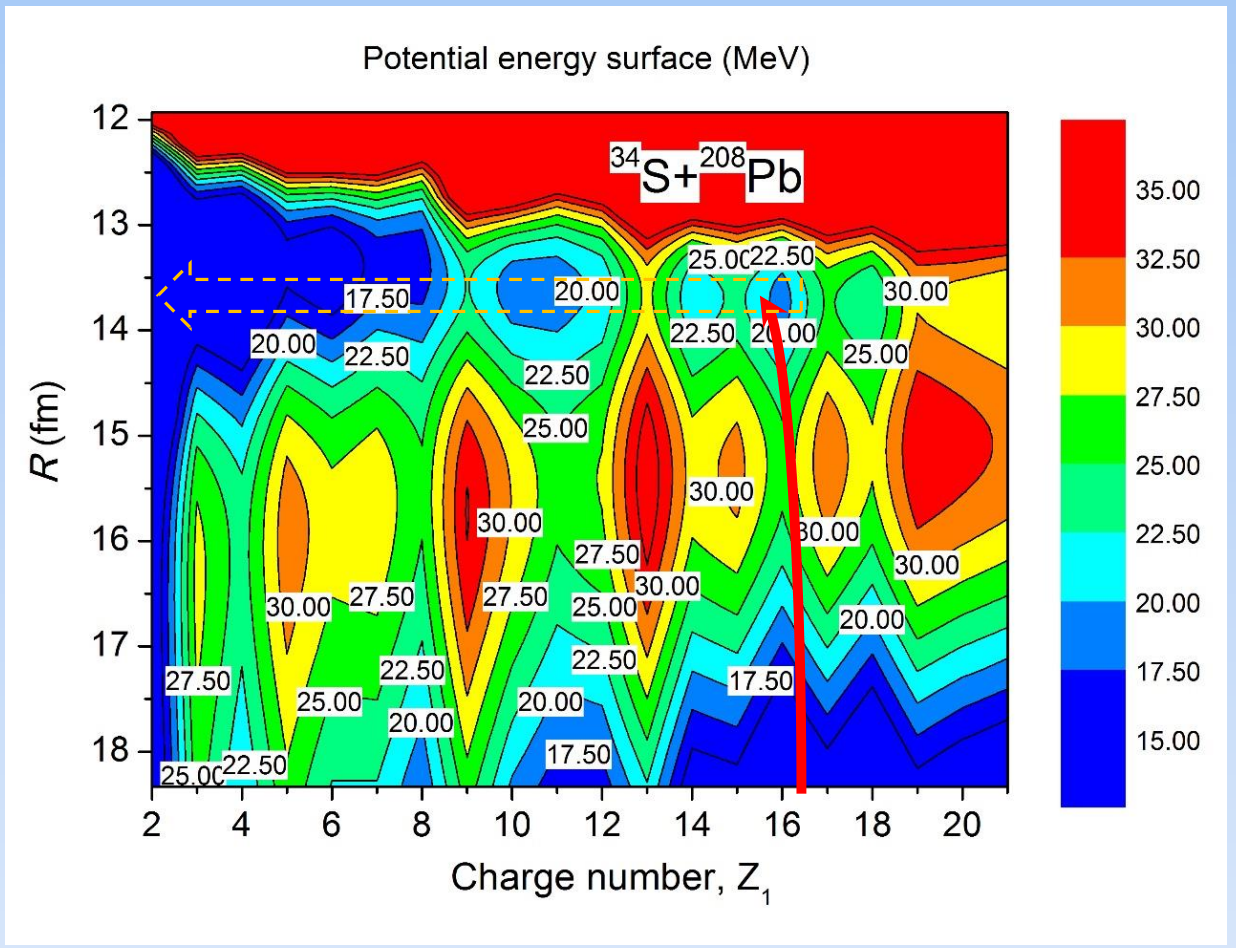

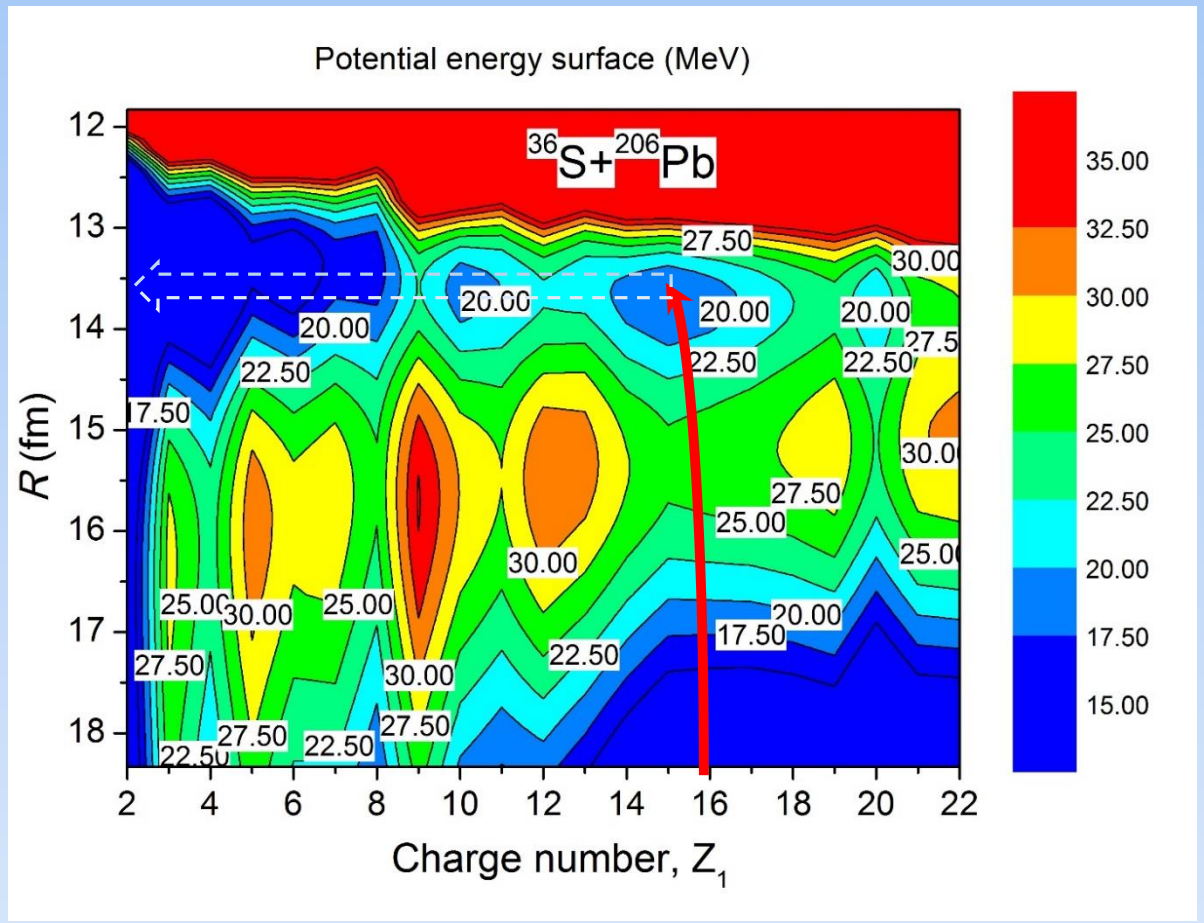

Reaction channels leading to yield of the binary products.

1. Quasifission

2.Incomplete fusion

Attempts to analyze the results of the mixed contributions of the fusion-fission and quasifission products

Meenu Thakur et al., Eur. Phys. J. A (2017) **53**: 133

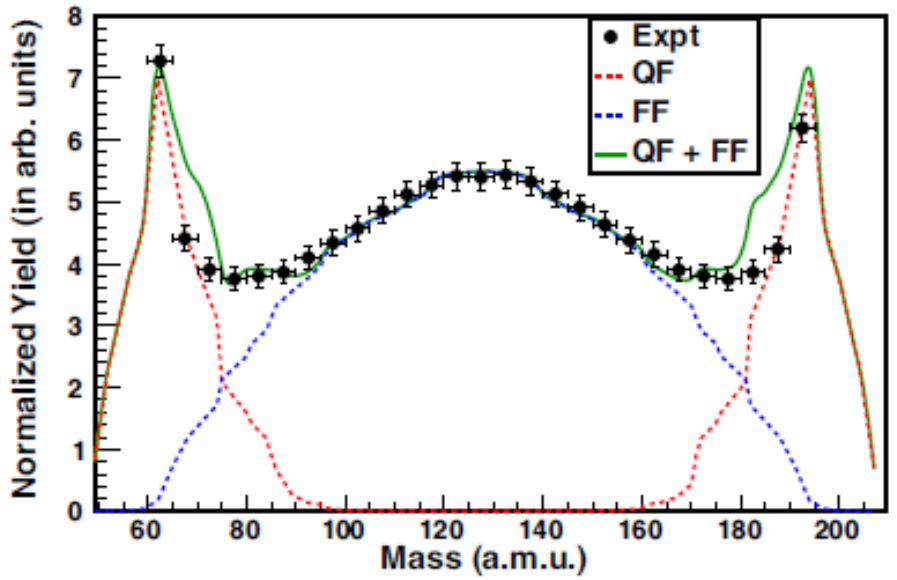

Fig. 7. (Color online) The results of the theoretical estimations of the QF (red dashed curve) and FF (blue dashed curve) products in the framework of the DNS model [50] for the ^{48}Ti + ^{208}Pb reaction. The solid curve shows the sum of the both yields. The solid circle represents the normalized experimental mass yield.

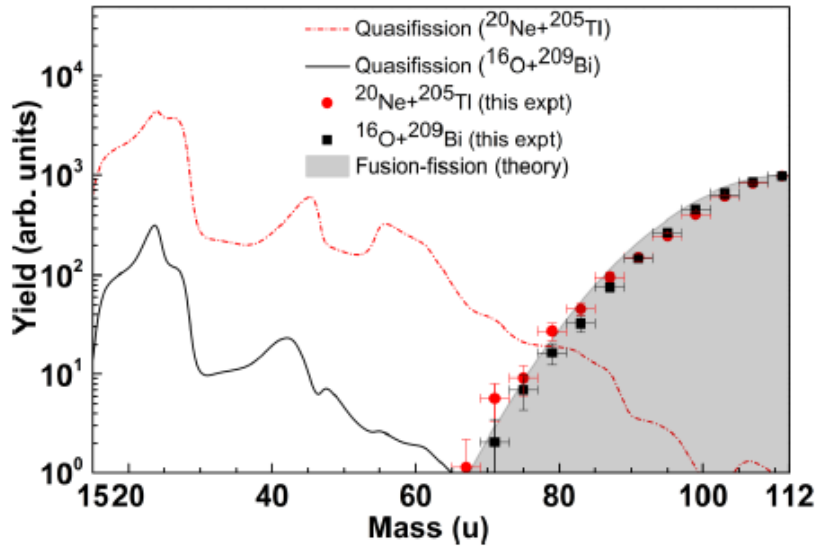

FIG. 7. Calculated mass distributions up to the symmetric mass ($A_{CN}/2 \approx 112$) at the excitation energy ≈83 MeV. The normalized fusion-fission yield (produced in both reactions) is shown by the shaded area and have been compared with the experimental data. The quasifission yields for ^{20}Ne + ^{205}Tl and ^{16}O + ^{209}Bi reactions are shown by dashed (blue) and solid (red) lines, respectively.

Nasirov, A. K., B. M. Kayumov, O. K. Ganiev and G. A. Yuldasheva . "A new dynamical mechanism of incomplete fusion in heavy-ion collisions." Physics Letters B 842: 137976 (2023).

Study Of Some Nuclear Reactions Induced by Heavy Ions at Intermediate Energies

ABSTRACT OF THE THESIS

SUBMITTED FOR THE AWARD OF THE DEGREE OF

DOCTOR OF PHILOSOPHY
IN
PHYSICS

BY
MUNTAZIR GULL

Under the Supervison of
PROF. ISAR AHMAD RIZVI

DEPARTMENT OF PHYSICS
ALIGARH MUSLIM UNIVERSITY
ALIGARH (INDIA)
2019

W.J. Knox, A.R. Quinton, C.E. Anderson, Phys. Rev. 120 (1960) 2120

PHYSICAL REVIEW VOLUME 120, NUMBER 6 DECEMBER 15, 1960

Evaporation of Charged Particles from Highly Excited Compound Nuclei*

W. J. KNOX,† A. R. QUINTON, AND C. E. ANDERSON
Yale University, New Haven, Connecticut

(Received July 6, 1960)

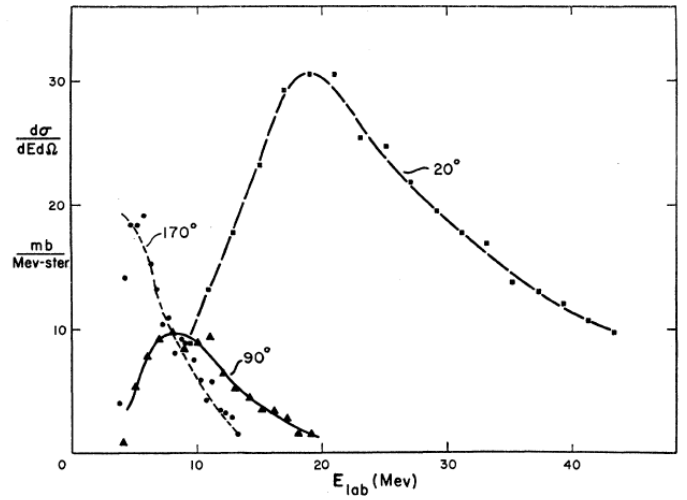

FIG. 1. Energy spectra of alpha particles emitted in the interaction of 160-Mev oxygen ions with Ni target nuclei. Spectra observed at three widely separated laboratory angles are shown. The shift in the energies of the particles with angle shows the large effect of the center-of-mass motion.

Role of the orbital angular momentum in the reaction mechanism.

$$\overrightarrow{L_1} = [\overrightarrow{b_1} \times \vec{P}]$$

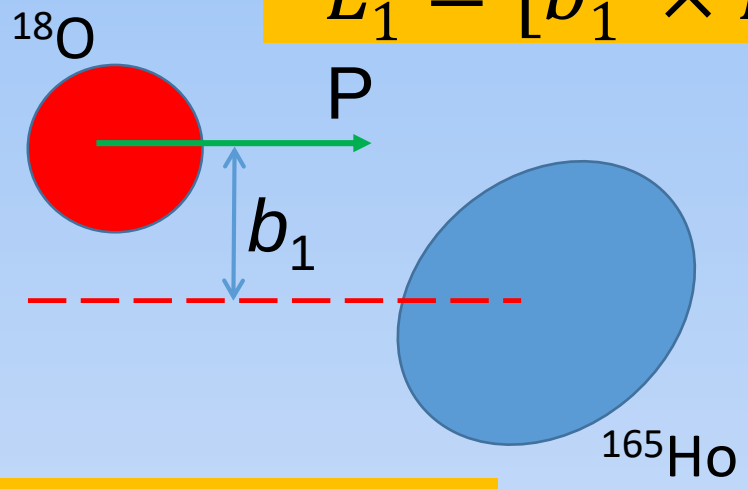

$$b_1 > b_2$$

$$\overrightarrow{L_2} = [\overrightarrow{b_2} \times \vec{P}]$$

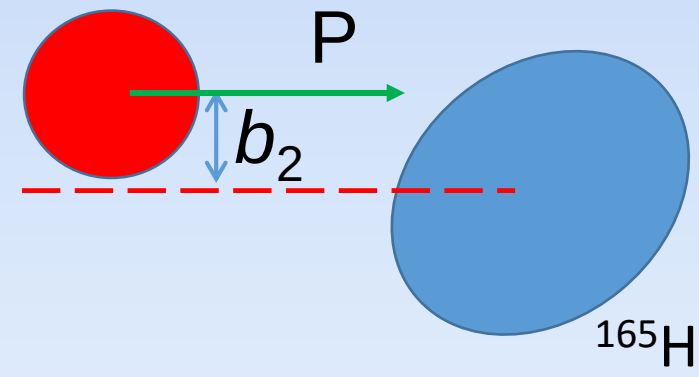

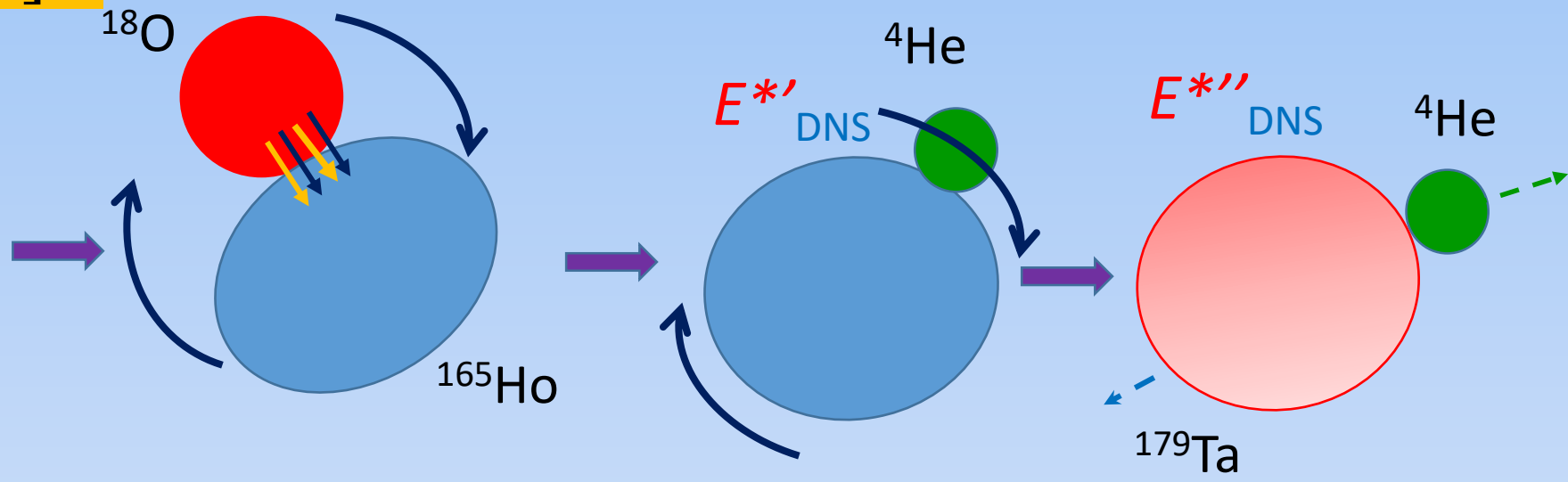

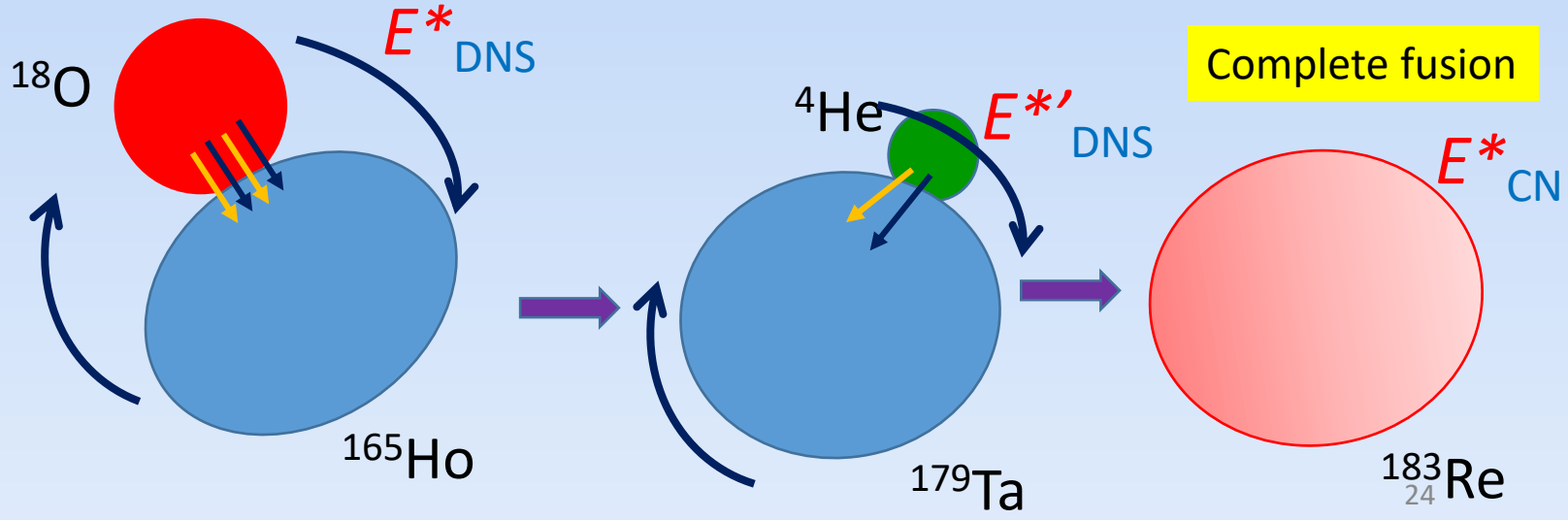

A.K. Nasurov et al. Physics Letters B 842: 137976 (2023)

$$\overrightarrow{L_1} = [\overrightarrow{b_1} \times \vec{P}]$$

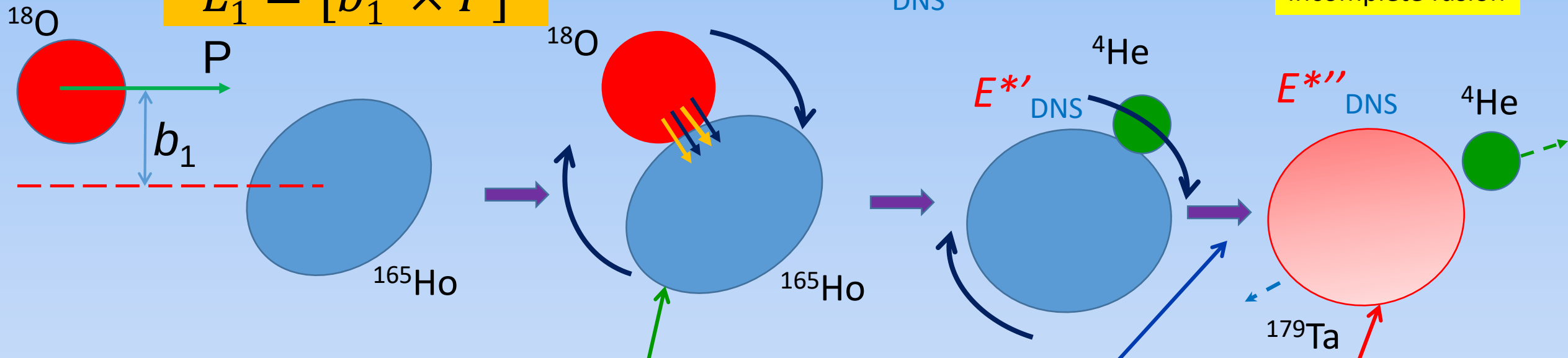

Calculation of the incomplete fusion cross section

$$\sigma_{icf}(E_{\mathrm{Lab}}, Z) = \sum_{l=0}^{l_a} \sigma_{cap}(E_{\mathrm{Lab}}, l) Y_z(E_{\mathrm{Lab}}, l) Wsur(E_{\mathrm{Lab}}, l, Z)$$

The role of the orbital angular momentum

$U(Z,A,L,R)=V_{coul}(Z,A,R)+V_{nucl}(Z,A,R,L)+V_{rot}(Z,A,R,L)+Q_{gg}(Z,A)-V_{rot}^{(CN)}(L)$

$$V_{rot}(Z,A,R_{min},L)=\frac{l(l+1)\hbar^2}{2J_{DNS}(Z,A,R_{min})}$$

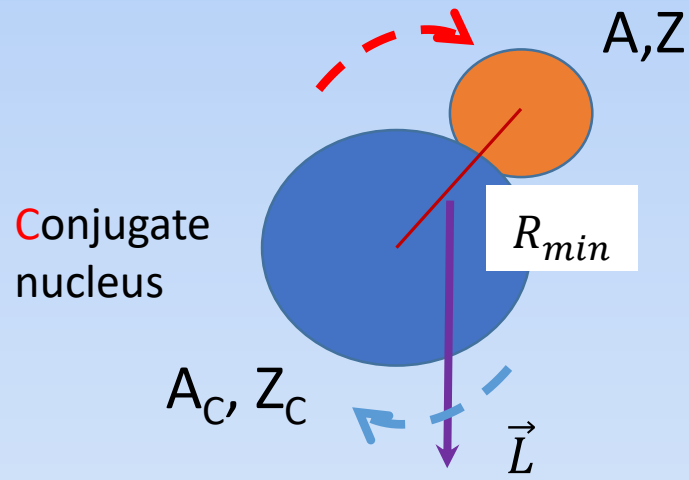

$$J_{DNS}(Z,A,R_{min})=\mu_Z R_{min}^2+\left(J_1(Z,A)+J_2(Z_C,A_C)\right)/2$$

$^{16}O+^{130}Te$

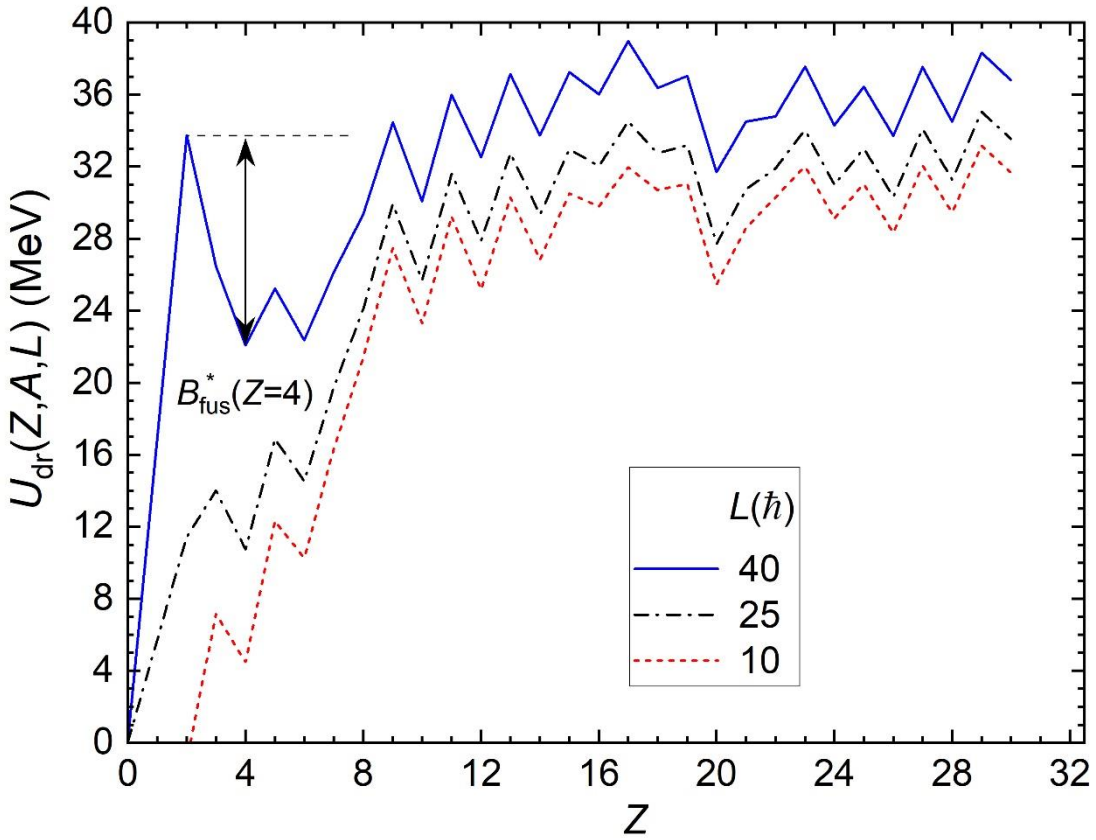

Driving potential

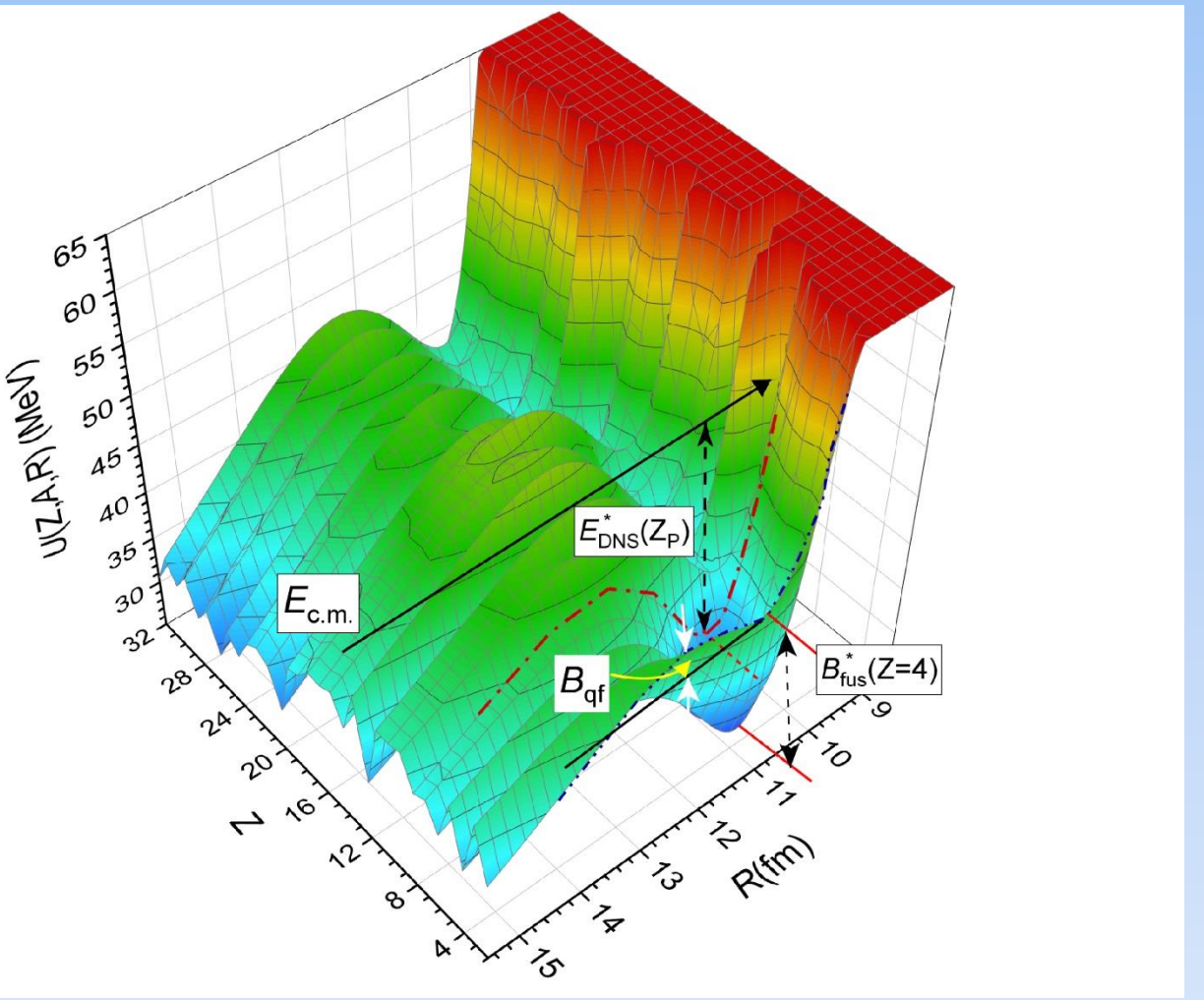

Potential energy surface

Appearance of the hindrance to complete fusion Phys. Lett. B 842: 137976 (2023)

$$E^*_{DNS}(Z)=E_{c.m.}-V_{min}+(B_P+B_T)-(B_Z+B_{ztot-z})$$

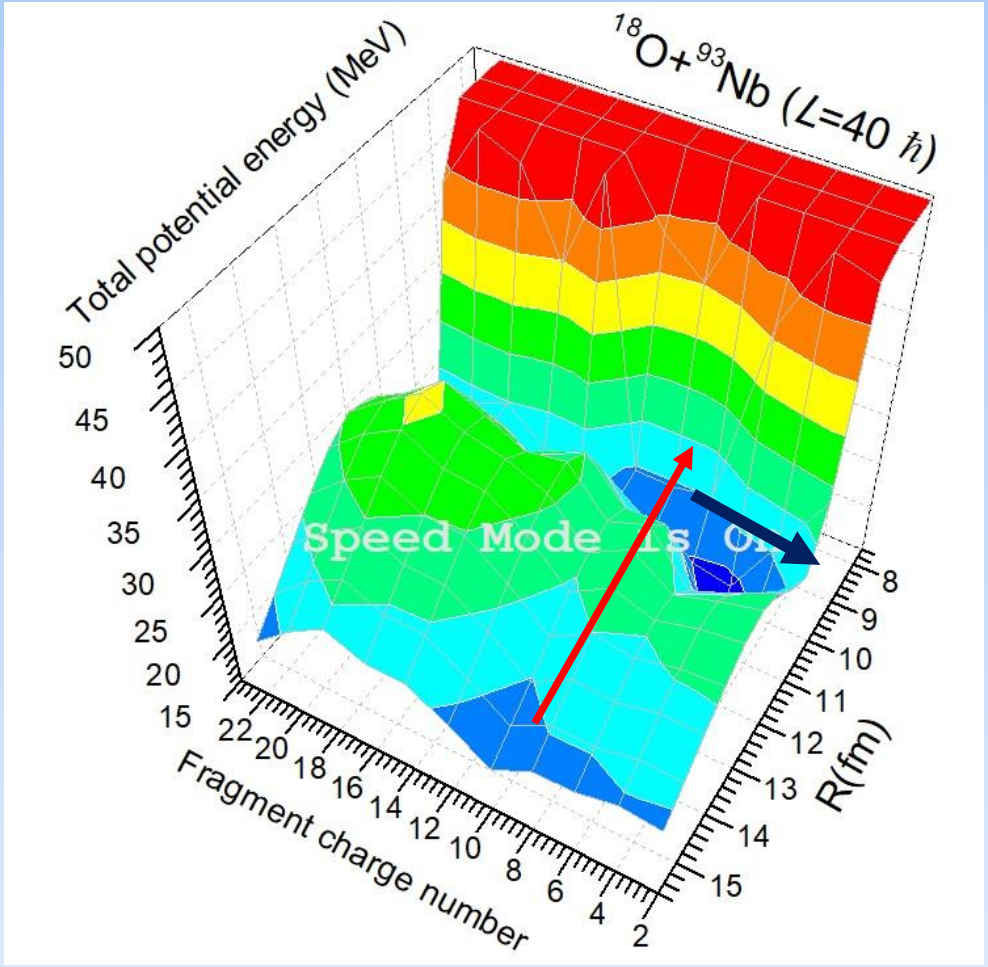

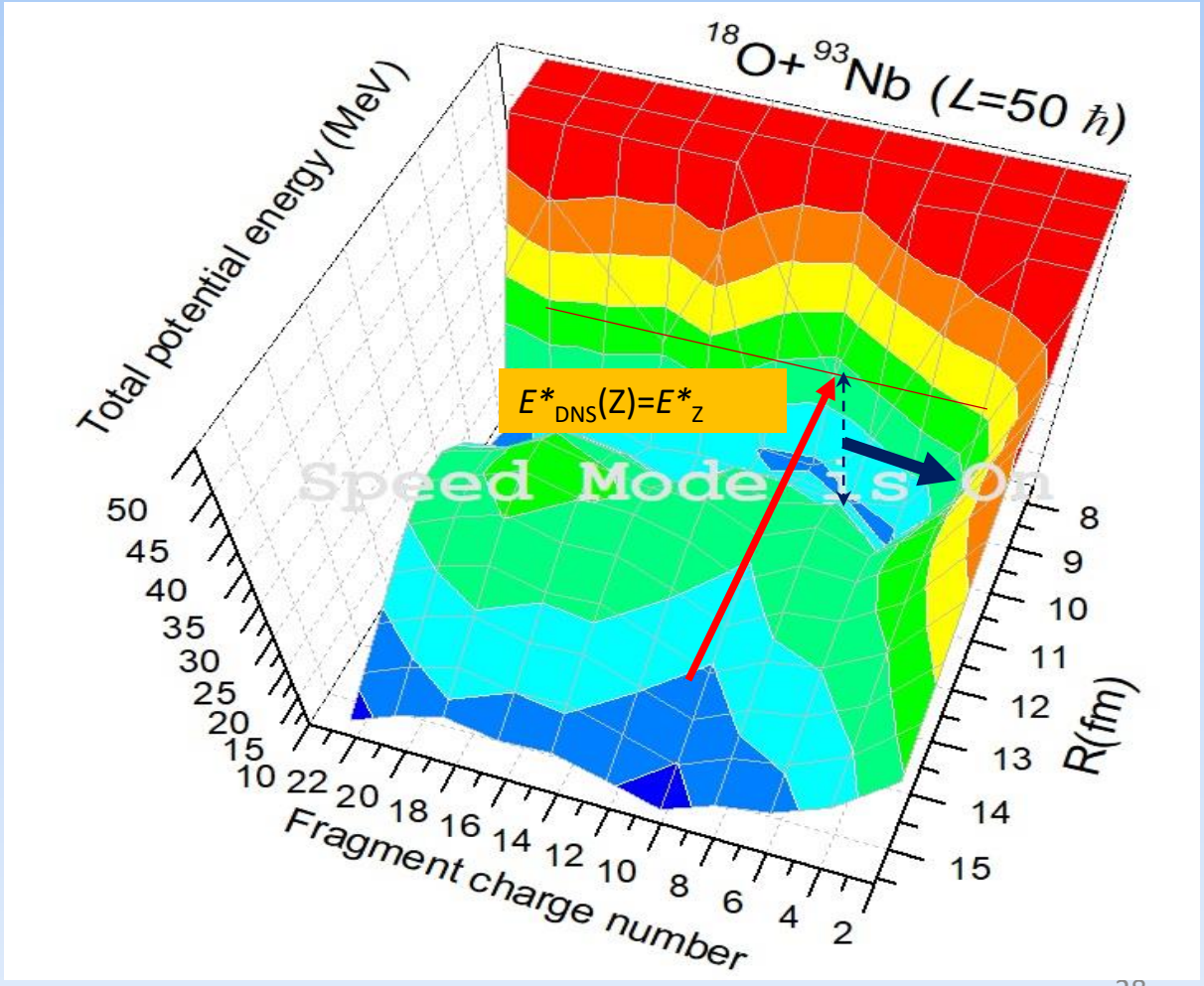

Solutions of the transport master equations for the evolution and decay dinuclear system formed in reaction $^{18}O+^{165}Ho$

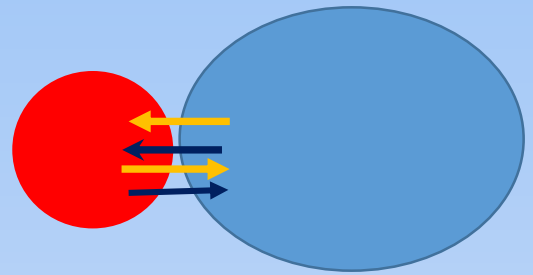

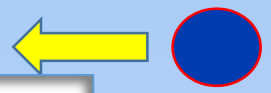

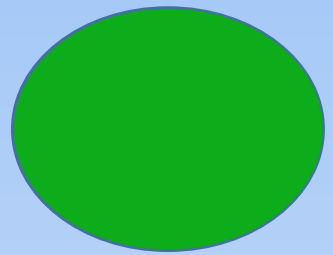

$$Y_Z(t) = \Lambda_Z^{qf} \int_0^t D_Z\ (t)dt$$

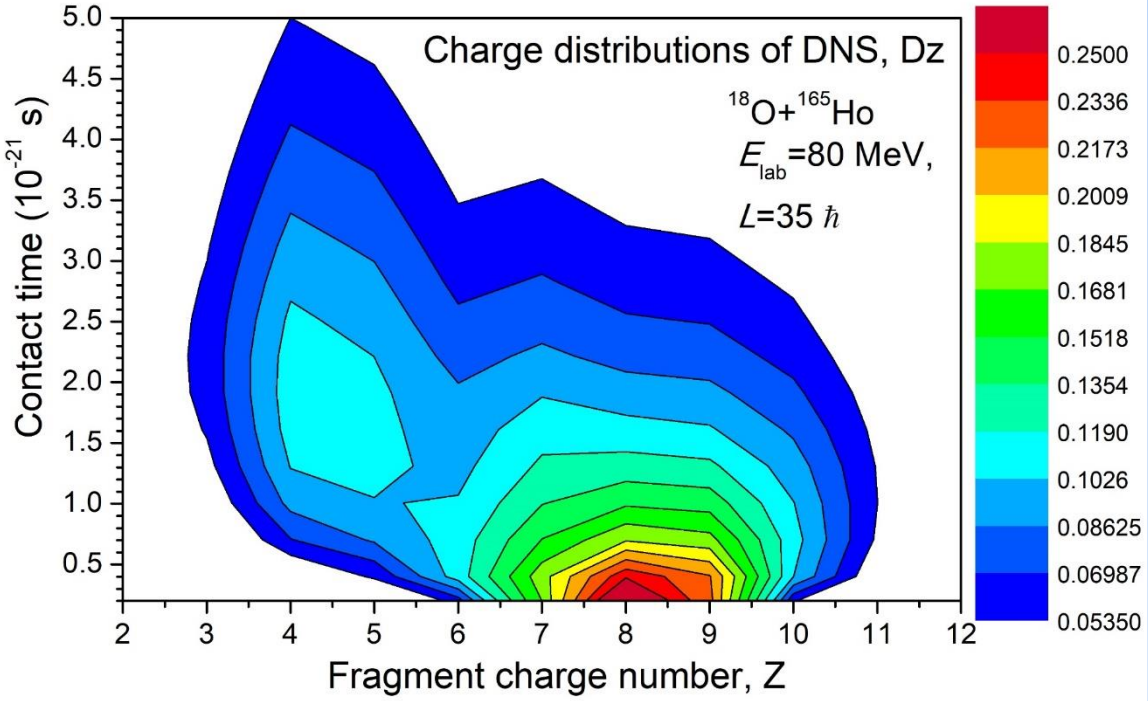

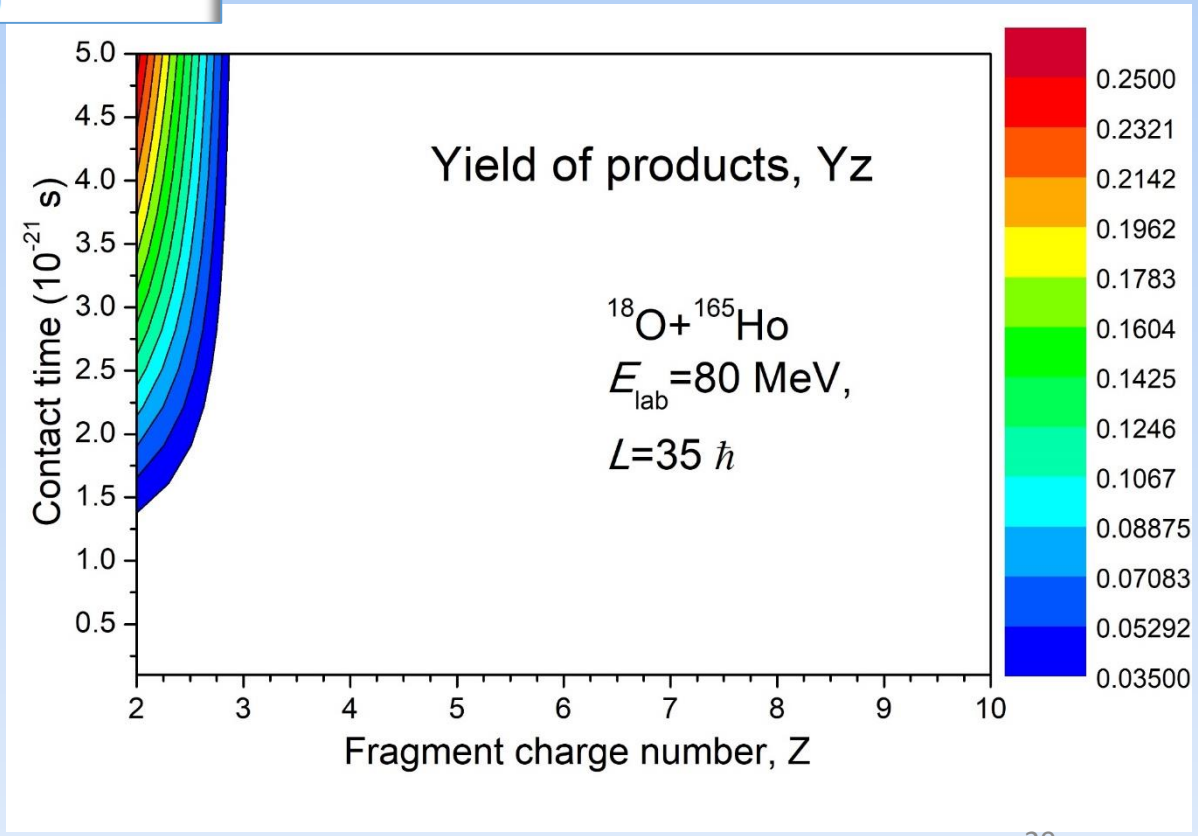

Comparison of the results by dinuclear system model and PACE4 code.

Theoretical result of this work

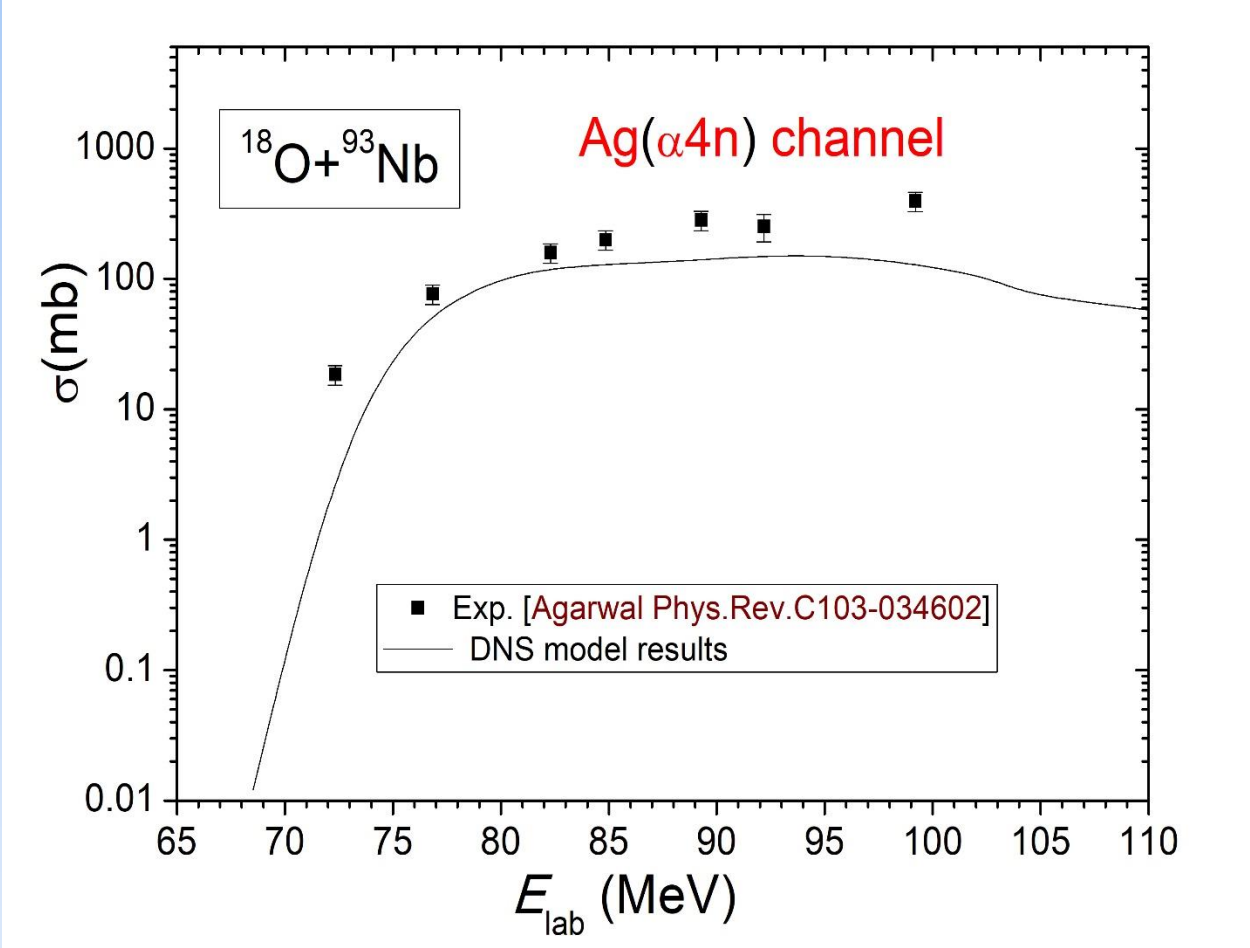

Avinash Agarwal, Phys.Rev.C103-034602 (2021)

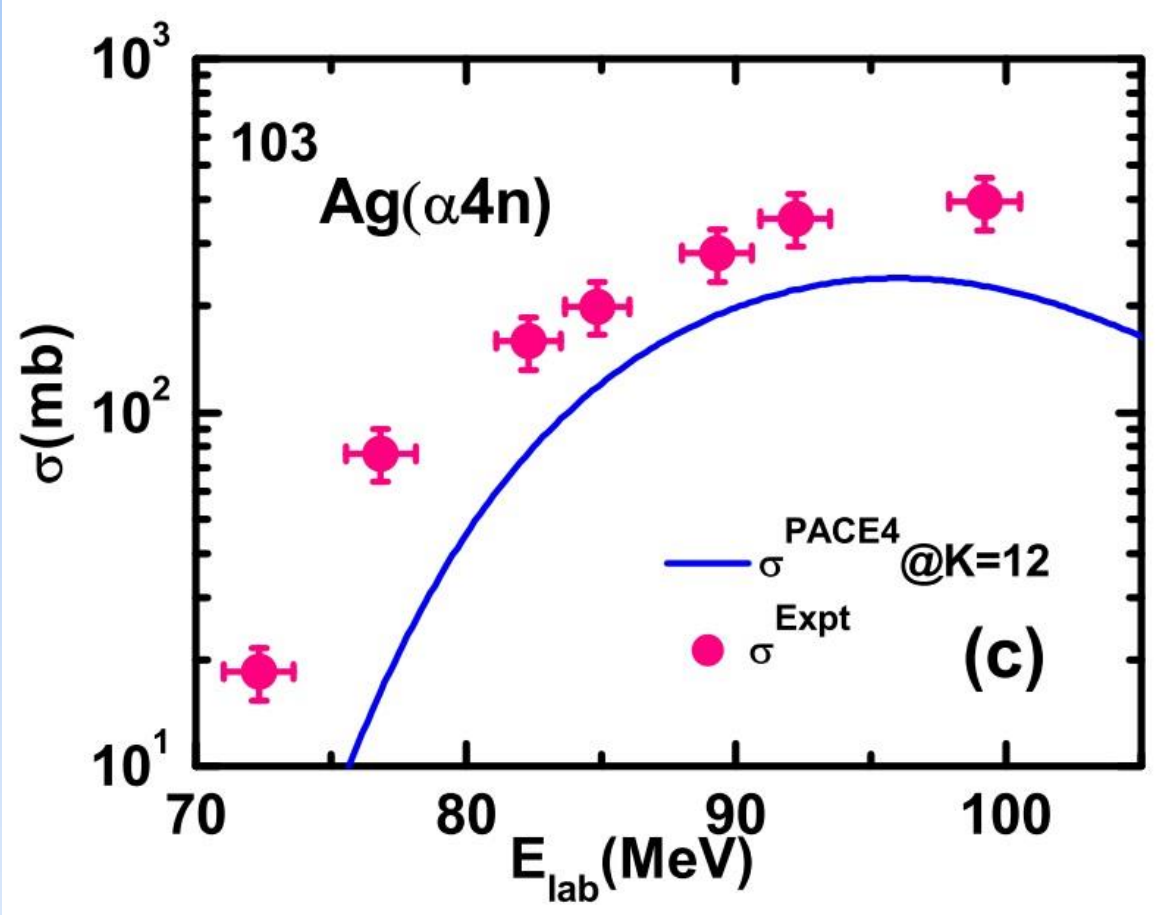

Comparison of the results by dinuclear system model and PACE4 code.

Theoretical result of this work

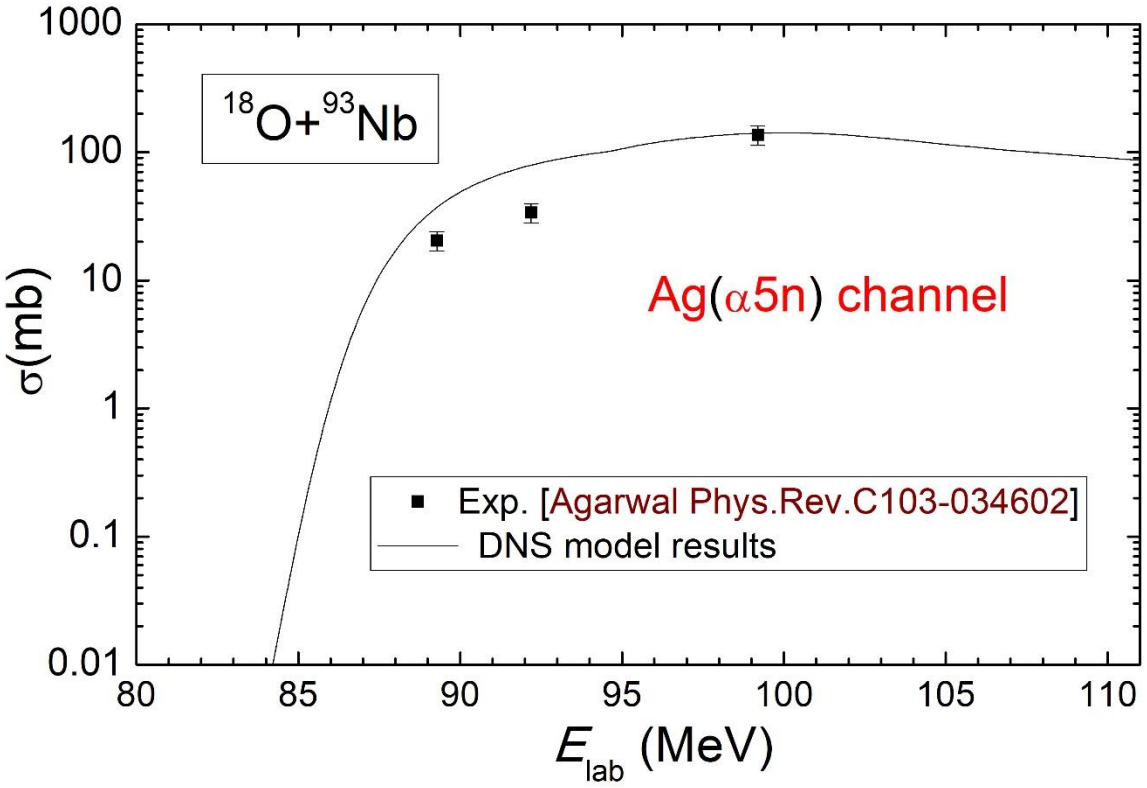

Avinash Agarwal, Phys.Rev.C103-034602 (2021)]

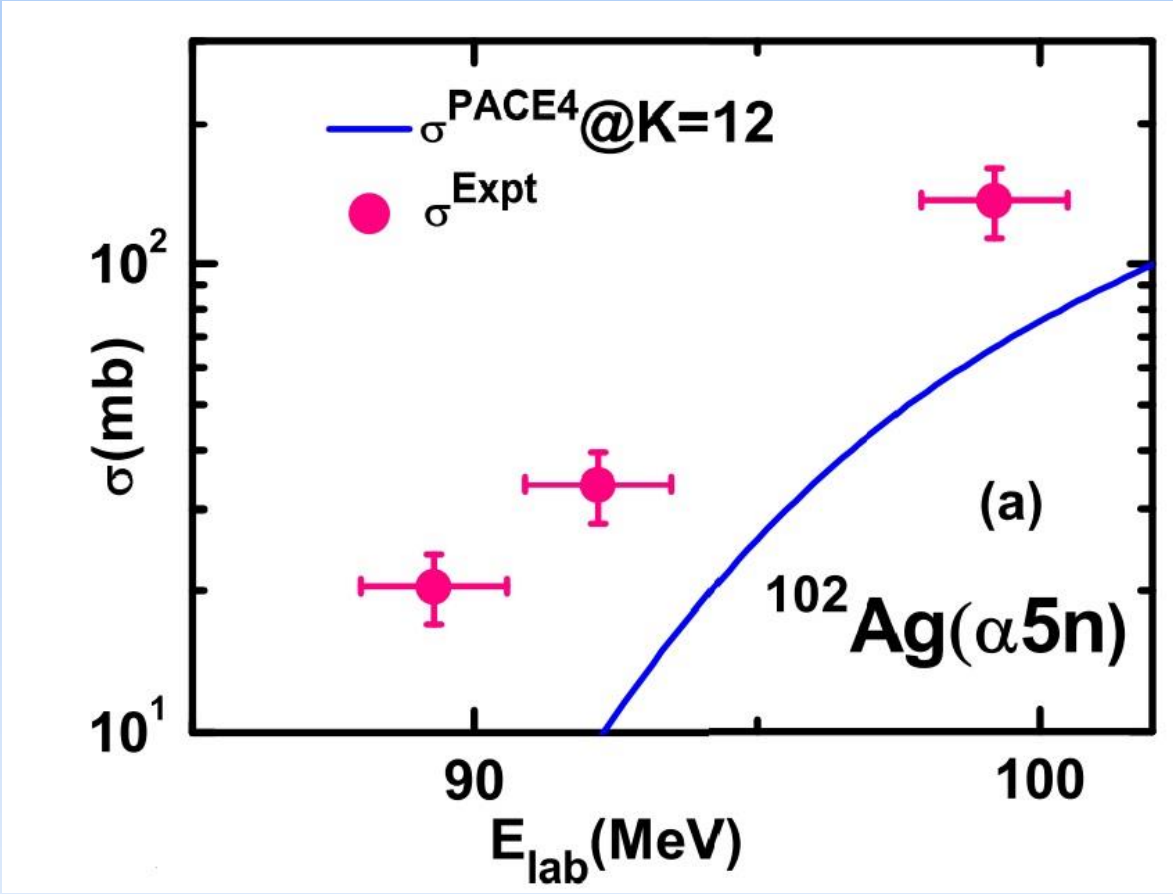

PHYSICAL REVIEW C **110**, 044610 (2024)

Measurements of evaporation residue cross sections and evaporation-residue-gated γ-ray fold distributions for the $^{32}S + ^{154}Sm$ system

R. Sariyal,[1,2,*,†] I. Mazumdar,[2,‡] D. Mehta,[1] N. Madhavan,[3] S. Nath,[3] J. Gehlot,[3] Gonika,[3] S. M. Patel,[2] P. B. Chavan,[2] S. Panwar,[4] V. Ranga,[4] A. Parihari,[5,§] A. K. Nasirov,[6,7] and B. M. Kayumov[7,8]

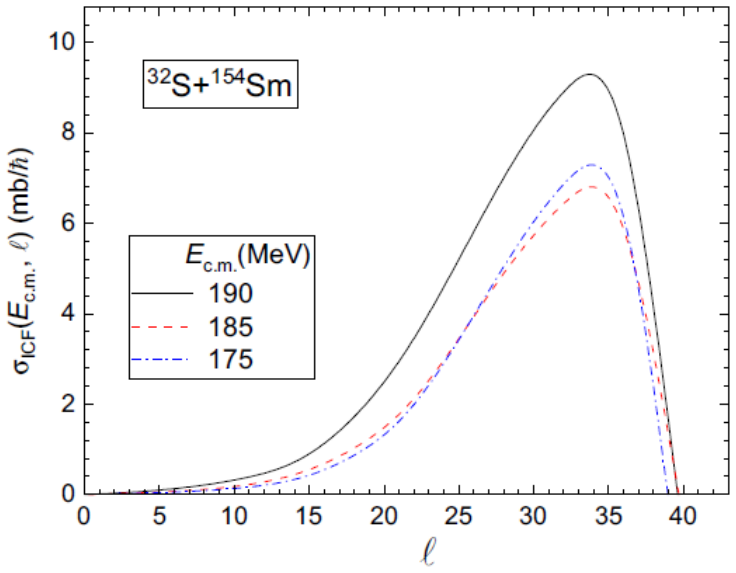

FIG. 16. The partial cross section of the incomplete fusion $[\sigma_{ICF}(E_{c.m.}, \ell)]$ calculated in this work for the $^{32}S + ^{154}Sm$ reaction as a function of the collision energy $E_{c.m.}$ and orbital angular momentum ℓ.

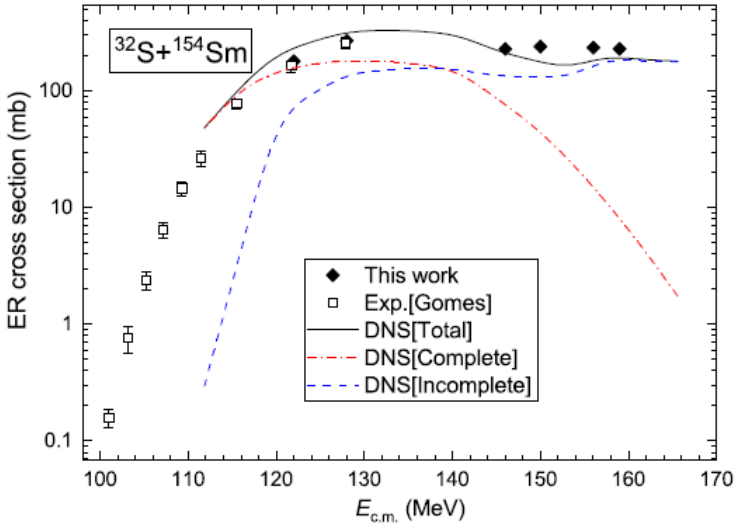

FIG. 17. Comparison of the theoretical (solid curve) and measured total cross sections of the evaporation residues formed in the $^{32}S + ^{154}Sm$ reactions. The filled diamonds and open squares present the experimental data of this work and the ones obtained from Ref. [14], respectively. The dashed and dot-dashed curves are contributions of the complete and incomplete fusion mechanisms estimated by the DNS model, respectively.

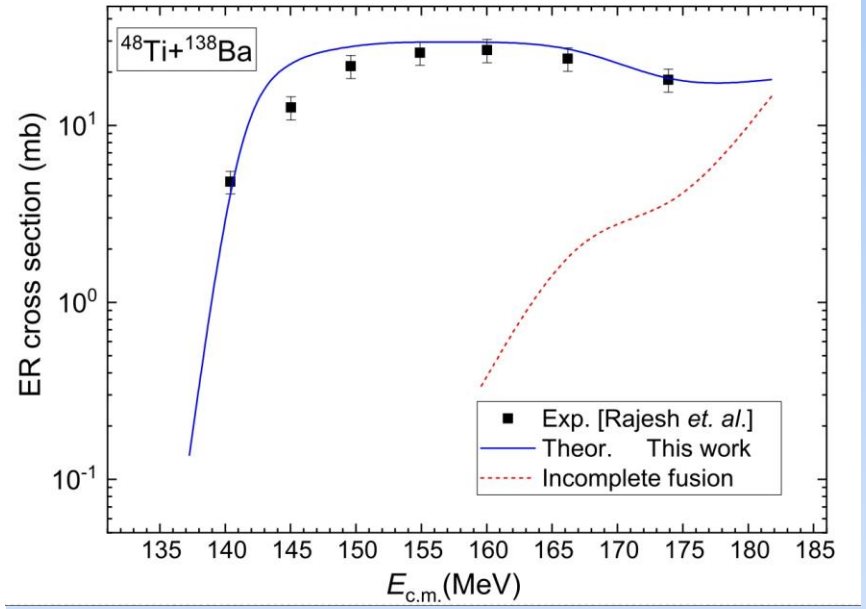

$$\sigma_{icf}(E_{\mathrm{Lab}}, Z) = \sum_{l=0}^{l_d} \sigma_{cap}(E_{\mathrm{Lab}}, l) Y_z(E_{\mathrm{Lab}}, l) Wsur(E_{\mathrm{Lab}}, l, Z)$$

Calculation of the evolution of the charge distribution between fragments of the dinuclear system

$$\frac{\partial D_Z(E_Z^*,l,t)}{\partial t} = \Delta_{Z+1}^{(-)} D_{Z+1}(E_Z^*,l,t) + \Delta_{Z-1}^{(+)} D_{Z-1}(E_Z^*,l,t) - \left(\Delta_Z^{(-)} + \Delta_Z^{(+)} - \Lambda_Z\left(B_{qf}^{(Z)}, T_Z\right)\right) D_Z(E_Z^*,l,t)$$

$$\Lambda_Z\left(B_{qf}^{(Z)}, T_Z\right) = \frac{\Gamma_Z}{2\pi}\frac{\omega_m}{\omega_{qf}} exp\left(\frac{-B_{qf}^{(Z)}}{T_Z}\right), \qquad \Gamma_Z = \sqrt{\left(\frac{\gamma}{2\mu_Z}\right)^2 + \omega_{qf}^2} - \frac{\gamma}{2\mu_Z}$$

$\gamma = 8 \cdot 10^{-22}$ MeV sec $^{-1}$

$$T_Z(A, L) = \sqrt{\frac{E_Z^*}{a}} \quad a = \frac{A_{tot}}{10}\ \text{MeV}^{-1}$$

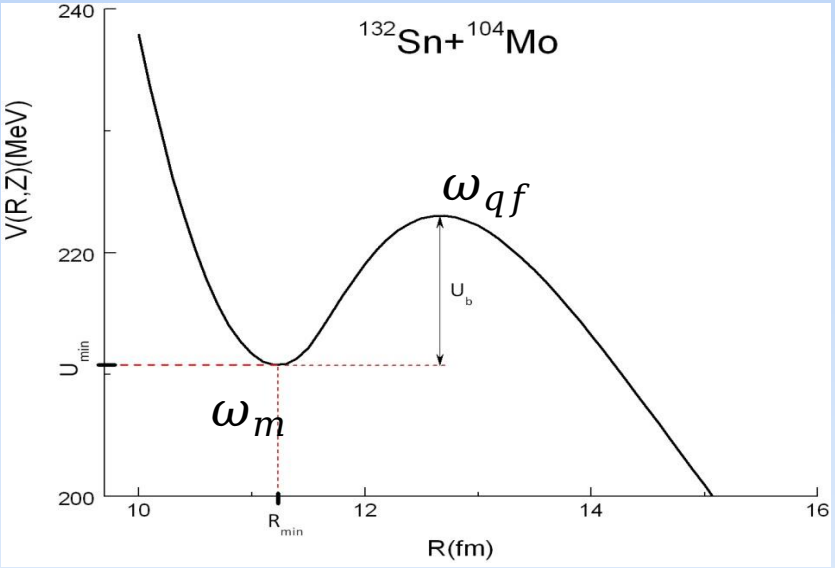

Nasirov A.K. et al. Nuclear Physics A 759 (2005) 342–369

Fazio G. et al, Modern Phys. Lett. A 20 (2005) p.391

Nucleon transfer coefficients for evolution of the charge asymmetry of dinuclear system

$$\Delta_Z^{(\pm)} = \frac{1}{\Delta t}\sum_{P_z,T_Z}\left|g_{P_zT_Z}\right|^2 n_{T_Z(P_Z)}(t)(1-n_{T_Z(P_Z)}(t))W_{P_zT_Z}(\Delta t) \Big/ (\varepsilon_{Pz} - \varepsilon_{Tz})^2$$

$$W_{P_zT_Z}(\Delta t) = (1 + e^{-2(\Gamma_{Pz}+\Gamma_{Tz})\Delta t/\hbar} - 2.\, e^{-2(\Gamma_{Pz}+\Gamma_{Tz})\Delta t/\hbar}\cos\left((\varepsilon_{Pz} - \varepsilon_{Tz})\Delta t/\hbar\right)$$

$$\frac{1}{\tau_i^{(\alpha)}} = \frac{\sqrt{2}\pi}{32\hbar\varepsilon_{F_K}^{(\alpha)}}\left[(f_K - g)^2 + \frac{1}{2}(f_K + g)^2\right]$$

$$\times\left[\left(\pi T_K\right)^2 + \left(\tilde{\varepsilon}_i - \lambda_K^{(\alpha)}\right)^2\right]\left[1+\exp\left(\frac{\lambda_K^{(\alpha)} - \tilde{\varepsilon}_i}{T_K}\right)\right]^{-1}, \quad \text{(A.1)}$$

where

$$\Gamma_i = \hbar/\tau_i \qquad T_K(t) = 3.46\sqrt{\frac{E_K^*(t)}{\langle A_K(t)\rangle}} \qquad \text{(A.2)}$$

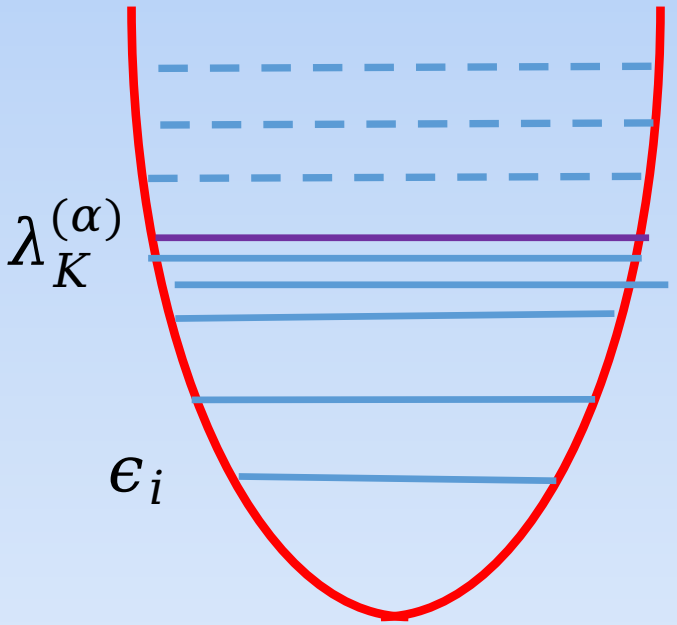

G.G. Adamian, et al. Phys. Rev. C**53,** (1996) p.871-879
R.V. Jolos et al., Eur. Phys. J. A **8, 115–124 (2000)**

Conclusion

1. The study of the different reaction channels in heavy ion collisions by the dinuclear system model allows us to find a reason of the hindrance for complete fusion of the mass symmetric nuclei.

2. The hindrance to fusion increases by the increase of the angular momentum of collision.

3. Complete fusion occurs by multinucleon transfer through the neck connecting two fragments of dinuclear system.

4. The incomplete fusion is a quasifssion in the region of the very asymmetric masses. Projectile nucleus breaks down after capture, not before capture.

The results have been obtained in cooperation with my young colleagues in Uzbekistan/

B.M. Kayumov[1,2], E.D. Khusanov[1,3], G.A. Yuldasheva[1]


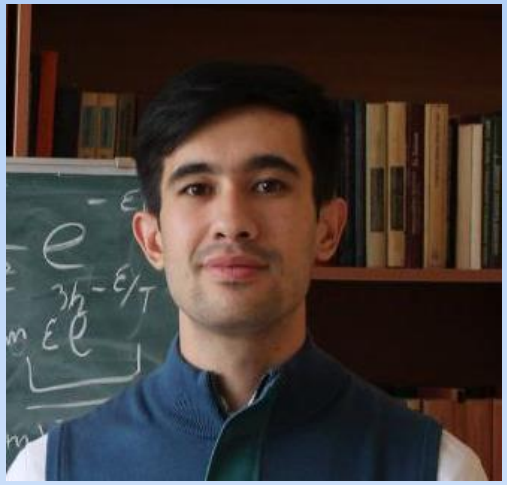


[1]Institute of Nuclear Physics, Academy of Science of Uzbekistan

[2]New Uzbekistan University, Tashkent, Uzbekistan

[3] National University of Uzbekistan, Tashkent